TECHNICAL INFORMATION SERIES

R65SD50

THE STRUCTURE OF THE VISCOUS HYPERSONIC SHOCK LAYER

L. GOLDBERG

SPACE SCIENCES LABORATORY

MISSILE AND SPACE DIVISION

GENERAL ELECTRIC

SPACE SCIENCES LABORATORY

THEORETICAL FLUID PHYSICS SECTION

THE STRUCTURE OF THE VISCOUS HYPERSONIC SHOCK LAYER

By

L. Goldberg

Work performed for the Space Nuclear Propulsion Office, NASA, under Contract No. SNPC-29.
This report first appeared as part of Contract Report DIN: 214-228F (CRD), October 1, 1965. Permission for release of this publication for general distribution was received from SNPO on December 9, 1965.

R65SD50
December, 1965

MISSILE AND SPACE DIVISION

GENERAL ELECTRIC

CONTENTS

LIST OF FIGURES

16234

ABSTRACT

In this paper, a unified, theoretical model of the hypersonic viscous shock layer is presented, which, in a self-consistent manner, covers the entire range of shock Reynolds number from 0 (50) to 0 (10^4), including the effects of mass transfer. At the lowest Reynolds numbers considered, merging of the fully viscous shock layer with the shock wave occurs, and at the highest Reynolds numbers, the boundary layer asymptote is approached.

In addition, in order to compare the new results obtained from this new system of equations and boundary conditions at high Reynolds numbers with those obtained from boundary layer solutions for precisely the same hypersonic flight conditions, the boundary layer equations have been reformulated by retaining only first order terms in the above equations, in addition to making the usual assumption of a thin boundary layer. These equations and the boundary conditions used are equivalent to the more usual boundary layer formulation.

Correlated results of the numerical solutions obtained on a high speed digital computer (IBM 7094) for both systems of equations with their appropriate boundary conditions are presented. The range of hypersonic flight conditions for which calculations were obtained include flight velocities from 10,000 ft/sec. to 25,000 ft/sec.; altitudes from 100,000 ft. to 350,000 ft.; shock Reynolds numbers from order 10 to order 10^4; surface temperatures from $800^{\circ}R$ to $3500^{\circ}R$; and dimensionless mass transfer rate parameter f_w from 0 to -0.4. The correlations include non-similar heat transfer rates, skin friction and normal surface pressures.

Author

SYMBOLS

C_i	mass fraction of species i
C_{p_i}	specific heat of the i^{th} species at constant pressure
$\overline{C}_p$	frozen specific heat of mixture
$\mathcal{D}_{ij}$	binary diffusion coefficient
f	dimensionless stream function
h_i	static enthalpy of the i^{th} species, including chemical enthalpy
h	static enthalpy of the mixture
$\overline{h}$	dimensionless enthalpy
H	stagnation enthalpy
K_B	curvature of body
$\vec{n}$	outward normal unit vector
P	static gas pressure
Q	heat transfer
R_B	body radius
T	temperature
u, v	velocity components
$\overline{u}$, $\overline{v}$	dimensionless velocity components
$\vec{v}$	macroscopic gas velocity
$\vec{v}_i$	absolute velocity of species i
$\vec{V}_i$	diffusion velocity of species i
V_∞	flight speed
$\dot{w}_i$	chemical source term, net mass rate of production of species i per unit volume by chemical reaction
x, y, r	coordinate system
γ	ratio of specific heats
δ_{BL}	boundary layer thickness

δ_s shock detachment distance

Δ_s shock wave thickness

ϵ density ratio across shock wave

η transformed coordinate

μ viscosity

ρ density

τ shear stress

$\underset{\sim}{\tau}$ stress tensor

$\omega = \frac{X}{R_B}$ body coordinate angle

Subscripts

BL boundary layer

i i^{th} species

o in the absence of mass transfer

s behind an equivalent normal shock wave

SI shock interface

w wall, surface of vehicle

∞ upstream, ambient conditions

η denotes differentiation with respect to η

Dimensionless Groups

$$B = \frac{\dot{m}\,(H_s - h_w)}{Q_{w_o}}, \text{ mass transfer parameter}$$

$$C_H = \frac{Q_w}{\rho_\infty V_\infty (H_s - h_w)}, \text{ Stanton number}$$

$$C_f = \frac{\tau_w}{1/2\,\rho_\infty V_\infty^2}, \text{ skin friction coefficient}$$

$$Le = \frac{\rho \overline{C}_p \mathcal{D}_{ij}}{k}, \text{ binary Lewis number}$$

$$Pr = \frac{\mu \overline{C}_p}{k}, \text{ Prandtl number}$$

$$Re_s = \frac{\rho_\infty V_\infty R_B}{\mu_s}, \text{ shock Reynolds number}$$

I. INTRODUCTION

In considering the problem of the entry of a nuclear rocket into a planetary atmosphere, one is interested in determining the forces and external heating acting over the outer surface if it enters intact, or the forces and heating experienced by the small particles which result if the rocket is deliberately exploded.

As an object of arbitrary size, traveling at hypersonic speeds, descends into the Earth's atmosphere from a sufficiently high altitude, it encounters a variety of environmental conditions. Interest in the different aspects of these phenomena has shifted from the earliest studies of meteor entry, to the motion and thermal response of the early ballistic reentry vehicles, to the present more sophisticated problems of maneuvering entry.

Some of the earliest studies, restricted to order of magnitude analyses, are summarized by Hayes and Probstein (Ref. 1), where the entire hypersonic flight regime was divided into seven subregimes from continuum to free molecule flow, including the boundary layer regime, vorticity interaction regime, viscous layer regime, incipient merged layer regime, fully merged layer and transitional layer regimes, first order collision theory regime, and free molecule flow regime. In subsequent studies by Goldberg and Scala (Refs. 2 and 3), the number of major subregimes was reduced from seven to five by including all departures from the classical boundary layer regime, up to, but not including, the transitional regime, into a single classification called the low Reynolds number regime, which was then subdivided into the viscous layer regime and the merged viscous layer regime. In the present study, the required classification scheme is further reduced by no longer making a distinction between the two subregimes at low Reynolds number. That is, now a single system of equations and boundary conditions covers the entire hypersonic low Reynolds number flight regime.

The present classification scheme is shown in Figure 1 superimposed on typical ballistic and lifting trajectories. Note that Figure 1 is for a nominal nose radius of one tenth of a foot; for smaller nose radii, all of the

low density effects are shifted to lower altitudes. This decrease in altitude is approximately fifty thousand feet for each order of magnitude decrease in nose radius. Descriptive stagnation region profiles are shown to the right of the respective flight regimes.

Details of many of the phenomena encountered in the free and near free molecule regimes and transitional regimes can be found, for example, in references 4-12. Of primary concern in this paper is hypersonic continuum fluid mechanics in the forward region of a vehicle with emphasis on low Reynolds numbers.

II. DISCUSSION OF THE HYPERSONIC CONTINUUM FLOW FIELD

For the model employed in this study, it will be seen that the hypersonic flow field in the forward stagnation region can be characterized by three dimensionless quantities: 1) Re_s, the shock Reynolds number, defined as

$$Re_s = \frac{\rho_\infty V_\infty R_B}{\mu_s} \tag{1}$$

primarily accounts for the altitude and vehicle size since the ratio V_∞ / μ_s is relatively insensitive at hypersonic speeds; 2) ϵ, the density ratio across a normal shock wave, or

$$\epsilon = \frac{\rho_\infty}{\rho_s} \tag{2}$$

primarily accounts for the Mach number; and 3) Pr, the Prandtl number, defined as

$$Pr = \frac{\overline{C}_p \mu}{k} \tag{3}$$

accounts for the mode of energy transport.

At low altitudes (high Reynolds numbers) the flow field about a vehicle flying at hypersonic speeds is usually handled in a manner analogous to that suggested by Prandtl (Ref. 13). Of course, for hypersonic speeds, Prandtl's concept has been greatly broadened to include not only the transport of mass and momentum, but in addition, the transport of chemical species (diffusion) and energy. Furthermore, since the flow is supersonic, the two regions of inviscid flow are separated by a shock wave. Thus, the flow field about a vehicle traveling at hypersonic speeds and high Reynolds numbers is obtained theoretically by patching together the solutions of four separate and distinct regions of the flow field. That is, between the undisturbed free stream and the vehicle surface there are three more distinct regions of flow, namely the shock wave separated from the boundary layer by an inviscid region. In other words, at high Reynolds numbers the flow field tends to relax such that in most of the volume of the flow region the flow is relatively inviscid,

and only in regions with small dimensions do most of the properties of the flowing fluid change by relatively large amounts. Since the principle changes occur over small distances, the gradients there must be large. This, then, is the rationale of classical hypersonic continuum fluid mechanics.

For suborbital flight speeds, the radiative transport of energy is very small compared with the aerodynamic heat transfer and hence the dominant energy, momentum and mass transfer processes can all be adequately analyzed by studying the phenomena within the boundary layer adjacent to the surface. This procedure has yielded many useful solutions to the thermal protection problem, e.g. Refs. 14-17.

As has already been indicated, the boundary layer approximation is applicable for high Reynolds numbers. With decreasing Reynolds number (increasing altitude and/or decreasing body size), departures from boundary layer theory predictions become evident. The region between those Reynolds numbers where departures become significant and those at which kinetic theory considerations become important has been given the name of the low Reynolds number regime. Two most important overall effects are noted: 1) Since at high Reynolds numbers the boundary layer thickness, δ_{BL}, varies as

$$\delta_{BL} \alpha \frac{1}{\sqrt{Re_{\delta_{BL}}}} \tag{4}$$

and the shock layer thickness δ_s remains essentially constant (Refs. 2 and 3), at a sufficiently small Reynolds number the condition

$$\frac{\delta_{BL}}{\delta_s} << 1 \tag{5}$$

no longer holds, i.e., the fluscid effects extend throughout a major portion of the shock layer. Furthermore, as shown in reference 3 the viscous layer thickness is less than that predicted by eq. (4) at these low Reynolds numbers. That is, this non-isentropic layer is thinner than boundary layer predictions and so the gradients are greater, manifested by the larger heat transfer rates and skin friction than that given by boundary layer predictions (Refs. 2, 3, 18-22).

This condition has been given various names, e.g., vorticity interaction and viscous layer regimes. 2) The shock wave thickness, Δ_s, varies as

$$\Delta_s \alpha \frac{1}{Re_{\Delta_s}} \tag{6}$$

However, at high Reynolds numbers

$$\frac{\Delta_s}{\delta_{BL}} << 1 \tag{7}$$

Thus, the thickening of the shock wave does not become significant until even lower Reynolds numbers. With decreasing Reynolds number, the thickening non-isentropic shock wave structure begins merging with the thickening non-isentropic viscous layer structure, eventually forming a single non-isentropic relaxation zone in which the two separate non-isentropic processes become intermingled and coupled. Thus, an even larger volume becomes available to relax all of the non-isentropic effects, thereby reducing these gradients. This is evidenced by the turn around in the increasing predictions of $Q_w / Q_{w_{BL}}$ and $\tau_w / \tau_{w_{BL}}$ with decreasing Reynolds numbers (Refs. 23-26). This is usually given the name of merged or incipient merged layer regime. In this paper a distinction is no longer made between the two regions, but all departures from boundary layer predictions out to where the thickened shock wave structure includes the shock layer are treated with a single consistent set of equations and boundary conditions to account for both of these effects, and is now simply called the low Reynolds number regime.

In this study it is assumed that the Navier-Stokes equations are the valid conservation relations for continuum fluid mechanics. If, in the shock layer, the Navier-Stokes equations are suitably expanded in a body-oriented coordinate system in the forward region of a two dimensional or axisymmetric body it can be shown that the order of magnitude of each term of the system fits mainly into one of eight categories. When the equations are normalized such that the terms of largest magnitudes are of order one, it is found that there

are three orders of magnitude for the influscid terms and five for the fluscid terms, namely (in descending orders of magnitude):

Influscid Terms

$$\begin{array}{c|c|c} \rho u \dfrac{\partial u}{\partial x} & \rho v \dfrac{\partial v}{\partial y} & \rho v \dfrac{\partial}{\partial y}\left(\dfrac{v^2}{2}\right) \\ 0\,(1) & 0\,(\epsilon) & 0\,(\epsilon^2) \end{array} \tag{8}$$

Fluscid Terms

$$\begin{array}{c|c|c|c|c} \dfrac{\partial}{\partial y}\left(\mu \dfrac{\partial u}{\partial y}\right) & \dfrac{\partial}{\partial y}\left(\mu \dfrac{\partial v}{\partial y}\right) & \dfrac{\partial}{\partial x}\left(\mu \dfrac{\partial u}{\partial x}\right) & \dfrac{\partial}{\partial x}(\mu v) & \mu\left(\dfrac{\partial v}{\partial x}\right)^2 \\ 0\left(\dfrac{1}{\epsilon Re_s}\right) & 0\left(\dfrac{1}{Re_s}\right) & 0\left(\dfrac{\epsilon}{Re_s}\right) & 0\left(\dfrac{\epsilon^2}{Re_s}\right) & 0\left(\dfrac{\epsilon^3}{Re_s}\right) \end{array} \tag{9}$$

where examples of terms are shown associated with the respective orders of magnitude and the appropriate characteristic lengths are the nose radius, R_B, for x, and the shock detachment distance, δ_s, for y; see Figure 2. Note: it has been shown (Refs. 2, 3, 21, 26, 27) that in the stagnation region

$$\delta_s = 0\,(\epsilon R_B) \tag{10}$$

For hypersonic flight speeds in the Earth's atmosphere

$$\epsilon \leq 0\,(0.1) \tag{11}$$

Thus, it is seen that at large shock Reynolds numbers the flow in the shock layer can be quite accurately characterized by the terms of order one. However, since it is usually of little inconvenience to include the other influscid terms, these are often included. In either case, this system of equations is called the Euler equations. The boundary conditions are given by the Rankine-Hugoniot relations behind the shock and the vanishing of the normal component of velocity at the wall. However, upon a closer examination of the physics in the immediate vicinity of the surface, one finds that the tangential component of velocity and temperature are not equal to that given by a solution of the Euler equations but are more closely related to the physicochemical interactions that occur at the surface. Therefore, in the neighborhood of the wall, the Navier-Stokes equations are re-examined. This time the appropriate

normal characteristic dimension chosen is the boundary layer thickness, δ_{BL}. Again the equations are normalized such that the largest is of order one. Then each of the terms fits into one of the following five categories:

$$0(1),\quad 0\left(Re_{\delta_{BL}}^{-1/2}\right),\quad 0\left(Re_{\delta_{BL}}^{-1}\right),\quad 0\left(Re_{\delta_{BL}}^{-3/2}\right),\quad 0\left(Re_{\delta_{BL}}^{-2}\right) \tag{12}$$

where $Re_{\delta_{BL}}$ is the Reynolds number based on the boundary layer thickness. It is noted that there is an equivalency of the terms in the shock layer and in the boundary layer (of course the equations are the same) as shown by the following:

Shock Layer		Boundary Layer
$O(1) + O\left(\frac{1}{\epsilon\, Re_s}\right)$	$\sim$	$O(1)$
$O(\epsilon) + O\left(\frac{1}{Re_s}\right)$	$\sim$	$O\left(\frac{1}{\sqrt{Re_{\delta_{BL}}}}\right)$
$O(\epsilon^2) + O\left(\frac{\epsilon}{Re_s}\right)$	$\sim$	$O\left(\frac{1}{Re_{\delta_{BL}}}\right)$
$O\left(\frac{\epsilon^2}{Re_s}\right)$	$\sim$	$O\left(\frac{1}{\sqrt{\left(Re_{\delta_{BL}}\right)^3}}\right)$
$O\left(\frac{\epsilon^3}{Re_s}\right)$	$\sim$	$O\left(\frac{1}{Re_{\delta_{BL}}^2}\right)$

(13)

As discussed previously, at hypersonic speeds and high Reynolds numbers the flow can be separated into four distinct regions. It is usually assumed that the free stream flow is uniform, and so the equations describing this region are of zeroth order. Each of the three remaining regions are usually described by first order equations. The Rankine-Hugoniot shock relations are a coupled set of algebraic equations relating the flow conditions in one inviscid region to that of another relatively inviscid region; the two flow

regions separated by a highly non-isentropic shock wave. Note, in the stagnation region the separated shock wave is highly curved, thus the flow behind it is rotational and thereby, non-isentropic. However, at high Reynolds numbers, the gradient of the entropy behind the shock wave is far less than the gradient of the entropy in the shock wave and so is often neglected. On the other hand, the vorticity in the shock layer is characterized by a gradient of the tangential velocity. This gradient is small in comparison with its counterparts in the boundary layer and shock wave and is usually neglected for boundary layer calculations. In fact, upon examination of the usual transformed boundary layer momentum equation, assuming similarity (Refs. 1, 14-17) i. e.

$$\left(\frac{\rho\mu}{\rho_e\mu_e} f_{\eta\eta}\right)_\eta + f f_{\eta\eta} + \beta\left(\frac{\rho_e}{\rho} - f_\eta^2\right) = 0 \tag{14}$$

with boundary conditions

@ $\eta = 0$

$$f(0) = f_w,\ f_\eta(0) = 0 \tag{15}$$

and as $\eta \to \infty$

$$f_\eta(\eta) \to 1.0 \tag{16}$$

It is seen that since

$$f_\eta = \frac{u}{u_e} \tag{17}$$

for $f_\eta(\eta)$ to asymptotically approach one as $\eta \to \infty$ then $f_{\eta\eta}$ must go to zero, i. e. the gradient of u approaches zero. In fact, since as $\eta \to \infty$, $\frac{\rho\mu}{\rho_e\mu_e} \to 1.0$, $\frac{\rho_e}{\rho} \to 1.0$, $f_\eta \to 1.0$, therefore, since f increases monotonically, in order to satisfy the differential equation as $\eta \to \infty$, $f_{\eta\eta} \to 0$ and also $f_{\eta\eta\eta} \to 0$. The problem is not that the gradient of the tangential component of velocity must go to zero at the "edge" of the boundary layer, but that u_e is computed from the Euler equations in the absence of the boundary layer. Thus, unless the boundary layer is truly very thin in comparison to the shock layer thickness, i. e.

$$\frac{\delta_{BL}}{\delta_s} <<< 1.0 \qquad (18)$$

the level of u_e could be sufficiently underestimated so that significant errors occur. In fact, it will be shown that even at a high shock Reynolds number of 15,000 the discrepancy in skin friction is thirty percent, due primarily to this cause. This effect is in addition to the effect of a thinner viscous layer than predicted by boundary layer theory. The thinner viscous layer probably partially alleviates the situation. Thus, it is a combination of a thinner non-isentropic layer producing larger gradients, plus a higher level at the edge producing even higher gradients for the tangential component of velocity that is manifested by the large increase in skin friction predictions above that obtained from boundary layer theory. It is noted that the difference between the stagnation enthalpy, H_e, and the enthalpy behind a normal shock, h_s, is

$$H_e - h_s = \epsilon^2 H_e \qquad (19)$$

Thus, the effect on heat transfer is primarily due to the thinner viscous layer and not to a large discrepancy of the value at the edge.

The purpose of this study was to investigate the effects due to low Reynolds numbers. In searching for appropriate boundary layer predictions, it was found that differences in the various predictions (e. g. Ref. 28) were of the order of the low Reynolds numbers effects at higher Reynolds numbers. In order to overcome this difficulty, the boundary layer equations and boundary conditions were reformulated so that solutions with identical fluid properties and flight conditions could be obtained. These boundary layer solutions were then compared with the more exact solutions of Scala and Gilbert and the agreement was reasonable. Furthermore, it was then possible to separate the effects of low Reynolds numbers.

It can be argued that at low Reynolds numbers the gas in the hypersonic shock layer should be closer to being frozen chemically than in local thermo-chemical equilibrium. However, in order to assess this effect properly it is necessary to perform calculations for a system of equations capable of simulating non-equilibrium chemistry coupled with the flow. Since this would represent

a very complicated theoretical model, certain approximations have been introduced herein. In particular, it has been assumed that one may utilize an equilibrium dissociated gas model if the final results are normalized properly. Furthermore, some calculations were carried out utilizing a non-dissociating perfect gas model. It was found that when properly normalized with respect to boundary layer solutions utilizing the same gas model, that the low Reynolds correlations presented herein are also valid for the non-dissociating perfect gas model, which serves to eliminate much of the arbitrariness of the gas model.

The governing equations utilized in the present analysis are the same as those used in Reference 3, i. e., the equations of change for the flow of a compressible chemically reacting binary gas mixture interacting with an injected gas. Included are the conservation equations of mass, momentum and energy. The diffusion equation was uncoupled by assuming a Lewis number of unity. Thus, the above system of equations which was treated consists of a coupled set of 4 non-linear partial differential equations of 7th order having split boundary conditions. For the low Reynolds number regime, all terms of order $1/Re_s$ and larger were retained. The method of separation of variables was used to reduce the governing equations to a set of 6 coupled non-linear ordinary differential equations of order 10 with an "unknown" range of integration.

The outer boundary conditions are similar to, but are more complete and consistent with the low Reynolds number equations described above, than those suggested in Reference 29 and utilized by Cheng (Ref. 25), Probstein and Pan (Refs. 30 and 31) and Kao (Ref. 26). These include the effects of transport of mass, momentum and energy in a thickened shock wave. It was also assumed that the shock wave was concentric with the body, i. e. thin shock layer approximation.

The remaining transport properties were evaluated by assuming the Prandtl number to be constant at a value of 0. 71 and the viscosity obeyed Sutherland's Law.

III. BASIC RELATIONS

In the absence of external force fields the steady state form of the Navier-Stokes equations is:

Conservation of Species i

$$\nabla \cdot (\rho_i \vec{v}_i) = \dot{w}_i \tag{20}$$

Conservation of Momentum

$$\rho(\vec{v} \cdot \nabla)\vec{v} = -\nabla p + \nabla \cdot \underset{\sim}{\tau} \tag{21}$$

Conservation of Energy

$$\rho \vec{v} \cdot \nabla \left(h + \frac{\vec{v} \cdot \vec{v}}{2}\right) = -\nabla \cdot \vec{Q} + \nabla \cdot (\underset{\sim}{\tau} \cdot \vec{v}) \tag{22}$$

Equation of State

$$\rho = \rho\,(h, p) \tag{23}$$

Summation of eq. (20) over all species yields the global continuity equation

$$\nabla \cdot (\rho \vec{v}) = 0 \tag{24}$$

Assuming continuity, uncoupled radiation, negligible pressure and thermal diffusion and Dufour effects, a binary mixture of chemically reacting "air molecules" and "air atoms" and a Lewis number of unity, the steady state form of the low Reynolds number equations in the absence of external force fields were derived in references 2 and 3 (i.e. retaining all terms from 0 (1) to 0 (Re_s^{-1})). These governing equations expanded for the coordinate system shown in Figure 2 are:

Continuity

$$\frac{\partial}{\partial x}(\rho u r^j) + \frac{\partial}{\partial y}(\rho v r^j) + \frac{\rho v r^j}{R_B} = 0 \tag{25}$$

x-Component of Momentum

$$\rho\left[u\frac{\partial u}{\partial x} + v\frac{\partial u}{\partial y} + \frac{uv}{R_B}\right] = -\frac{\partial p}{\partial x} + \left[\frac{\partial}{\partial y} + \frac{(2+j)}{R_B}\right]\left[\mu\frac{\partial u}{\partial y}\right] - \frac{1}{R_B}\frac{\partial}{\partial y}(\mu u) \tag{26}$$

y - Component of Momentum

$$\rho\left[u\frac{\partial v}{\partial x}+v\frac{\partial v}{\partial y}-\frac{u^2}{R_B}\right]=-\frac{\partial p}{\partial y}+\frac{2}{3}\frac{\partial}{\partial y}\left[\mu\left(2\frac{\partial v}{\partial y}-\frac{\partial u}{\partial x}-j\frac{u}{r}\right)\right]$$

$$+\frac{\partial}{\partial x}\left[\mu\frac{\partial u}{\partial y}\right]+j\frac{\mu}{r}\frac{\partial u}{\partial y} \tag{27}$$

Energy

$$\rho\left[u\frac{\partial H}{\partial x}+v\frac{\partial H}{\partial y}\right]=\left[\frac{\partial}{\partial y}+\frac{(1+j)}{R_B}\right]\left\{\frac{\mu}{Pr}\left[\frac{\partial H}{\partial y}+(Pr-1)\,u\frac{\partial u}{\partial y}\right]\right\}$$

$$-\frac{1}{R_B}\frac{\partial}{\partial y}(\mu u^2) \tag{28}$$

State

$$\rho=\rho\,(h,\ p) \tag{29}$$

Viscosity Law

$$\mu=\mu\,(h,\ p) \tag{30}$$

where H is the total enthalpy defined as

$$H=h+\frac{u^2+v^2}{2} \tag{31}$$

At this point then, there are six unknowns u, v, h, p, ρ and μ which may be determined by solving the six equations (25) through (30) simultaneously. Before discussing the boundary conditions the boundary layer equations will now be shown.

Retaining only first order terms and assuming that the boundary layer is very thin with respect to the shock layer thickness, the low Reynolds number viscous layer equations (eqs. (25) to (28)) can be reduced to the boundary layer equations, i. e.

Continuity

$$\frac{\partial}{\partial x}(\rho u r^j)+\frac{\partial}{\partial y}(\rho v r^j)=0 \tag{32}$$

x - Component of Momentum

$$\rho\left[u\frac{\partial u}{\partial x}+v\frac{\partial u}{\partial y}\right]=-\frac{\partial p}{\partial x}+\frac{\partial}{\partial y}\left[\mu\frac{\partial u}{\partial y}\right] \tag{33}$$

y - Component of Momentum

$$\frac{\partial p}{\partial y} = 0 \tag{34}$$

Energy

$$\rho \left[u \frac{\partial H}{\partial x} + v \frac{\partial H}{\partial y} \right] = \frac{\partial}{\partial y} \left\{ \frac{\mu}{Pr} \left[\frac{\partial H}{\partial y} + (Pr-1)\, u \frac{\partial u}{\partial y} \right] \right\} \tag{35}$$

Even though the term $\partial p/\partial x$ is of higher order, it is the usual practice to retain this term when studying the stagnation region, although Lees (Ref. 14) found it convenient to neglect the effects of the pressure gradient at the stagnation point.

IV. BOUNDARY CONDITIONS

Although it is recognized that slip effects at the wall may be quite important at the low Reynolds numbers considered in this paper, these effects have not been included in our present model. However, it has been indicated by Cheng (Ref. 32) that, "for a thin shock layer ($\epsilon \ll 1$) and a cold surface $\left(\frac{T_w}{T_{stag}} << 1\right)$ the velocity slip and temperature jump at the surface are small." Thus, we assume the usual no slip boundary conditions at the wall, i. e.

$$u(x, 0) = u_w(x) = 0 \tag{36}$$

$$v(x, 0) = v_w(x) \tag{37}$$

$$h(x, 0) = h_w(x) \tag{38}$$

The location of the edge of the viscous layer within the shock layer and the magnitude of the physical variables at the outer edge of the viscous layer are not known "a priori". Thus, in our previous studies (Refs. 2 and 3), which were primarily concerned with departures from boundary layer theory at relatively high Reynolds numbers, the low Reynolds number equations were integrated from the wall out to the discontinuous shock wave, where the physical variables could be calculated from the Rankine-Hugoniot shock relations. However, this investigation includes sufficiently small Reynolds numbers that the shock wave can no longer be considered thin enough to be treated as a discontinuity. Also, the shock layer may be fully viscous with no classical inviscid region separating the two distinct regions of flow characterized by large gradients of all of the fluid properties. The derivation of the Rankine-Hugoniot jump relations considers the conservation of mass, momentum and energy across a small region, in which very large changes take place completely within the small region. At the outer boundaries of the region it is necessary that the flow be influscid (i. e. the molecular transport phenomena within the moving fluid are negligible). Thus, the Rankine-Hugoniot shock relations are seen to become a poorer approximation with decreasing Reynolds number, since, like the boundary layer equations, they consist of only first

order terms, and require the flow outside to be relatively inviscid (of course, at the inner edge of the boundary layer, i.e., the wall, there is no fluid motion relative to the wall).

The problem is not that the Rankine-Hugoniot relations are invalid at these low Reynolds numbers. In fact, if a shock wave were somehow formed in an otherwise quiescent fluid for the same conditions, it would be found that sufficiently far removed from the shock wave the conditions on both sides were indeed related by the Rankine-Hugoniot relations. However, in the limited confines of the region of flow about the nose of a vehicle with a reasonable size, as the shock wave becomes thicker, its structure becomes more intimately coupled with that of the shock layer. Thus, it is no longer adequate to match only the flow variables, but one must also match the derivatives consistent with the mathematical order of the shock layer equations.

A scheme similar to that first suggested by Sedov et at. (Ref. 29) and utilized by Cheng (Ref. 25 and 32), Probstein and Pan (Refs. 30 and 31) and Kao (Ref. 26) has been used to obtain the proper outer boundary conditions for the low end of the low Reynolds number regime. In this scheme, one is still not concerned with the complete internal structure of the shock wave but only with the structure immediately before and after the region of maximum gradients. In the region of maximum gradients (called the shock wave) a valid model has yet to be demonstrated, however, adequate models can be constructed fore and aft of the shock wave and then related to one another by overall conservation considerations. Thus, we postulate the Navier-Stokes equations in both regions. Although the Navier-Stokes equations are being accepted as a reasonable model behind the shock wave, in the undisturbed flow at low Reynolds numbers, it may not be very reasonable. However, there is no restriction on the distance in front of the shock wave. Thus, it is assumed that sufficiently far upstream the flow is completely undisturbed, and we need only consider the level of the free stream flow variables. This is consistent with our quasi-steady state analysis.

For a thin shock wave, i. e.

$$\Delta_s \leq 0\ (\delta_s) \tag{39}$$

concentric with the body surface it can be shown (Ref. 29) that the conservation relations across the shock wave are:

Continuity

$$\rho_\infty \vec{V}_\infty \cdot \vec{n} = \rho_{SI} \vec{V}_{SI} \cdot \vec{n} \tag{40}$$

Momentum

$$\rho_\infty \vec{V}_\infty (\vec{V}_\infty \cdot \vec{n}) + p_\infty \vec{n} - \underset{\sim}{\tau}_\infty \vec{n} = \rho_{SI} \vec{V}_{SI} (\vec{V}_{SI} \cdot \vec{n}) + p_{SI} \vec{n} - \underset{\sim}{\tau}_{SI} \vec{n} \tag{41}$$

Energy

$$\rho_\infty (\vec{V}_\infty \cdot \vec{n}) \left(h_\infty + \frac{V_\infty^2}{2} \right) - (\underset{\sim}{\tau}_\infty \vec{n}) \cdot \vec{V}_\infty + \vec{q}_\infty \cdot \vec{n}$$

$$= \rho_{SI} (\vec{V}_{SI} \cdot \vec{n}) \left(h_{SI} + \frac{V_{SI}^2}{2} \right) - (\underset{\sim}{\tau}_{SI} \vec{n}) \cdot \vec{V}_{SI} + \vec{q}_{SI} \cdot \vec{n} \tag{42}$$

where $\vec{n}$ is the outward unit normal vector, therefore

$$\vec{V} \cdot \vec{n} = v \tag{43}$$

is the normal component of velocity. The subscript SI refers to the shock interface, i. e. the surface at which the structure of the shock wave is matched with that of the shock layer. Thus, utilizing the same coordinate system and assumptions used in deriving the low Reynolds number viscous layer equations (eqs. (25) to 28)), plus assuming uniform flow in front of the shock wave, the modified shock jump relations become

Continuity

$$\left\{ \rho v \right\}_\infty = \left\{ \rho v \right\}_{SI} \tag{44}$$

x - Component of Momentum

$$\left\{ \rho v u \right\}_\infty = \left\{ \rho v u - \mu \left(\frac{\partial u}{\partial y} - \frac{u}{R_B} \right) \right\}_{SI} \tag{45}$$

y - Component of Momentum

$$\left\{\rho v^2 + p\right\}_\infty = \left\{\rho v + p + \frac{2}{3}\mu\left[\frac{\partial u}{\partial x} + j\,\frac{\cot(K_B x)}{R_B}\,u - 2\,\frac{\partial v}{\partial y}\right]\right\}_{SI} \tag{46}$$

Energy

$$\left\{\rho v\left(h + \frac{V^2}{2}\right)\right\}_\infty = \left\{\rho v\left(h + \frac{u^2+v^2}{2}\right) - \frac{\mu}{Pr}\frac{\partial h}{\partial y} - \mu u\left(\frac{\partial u}{\partial y} - \frac{u}{R_B}\right)\right\}_{SI} \tag{47}$$

Note that the x-component of momentum does not yield $u_\infty = u_{SI}$ except at very high Reynolds numbers.

Those terms with a coefficient of viscosity are of order Re_s^{-1}. So it is seen, that as expected, in the high Reynolds number limit we recover the usual Rankine-Hugoniot shock relations, and the order of the boundary conditions is consistent with the differential equations. Note: the shock curvature is included in the shock boundary conditions.

The low Reynolds number viscous layer partial differential equations are of order seven requiring seven boundary conditions given by eqs. (36) to (38) and eqs. (44) to (47).

The location of the shock interface, or the surface where the matching of the two structures occurs, can be determined by the following constraint based on the conservation of mass:

$$\rho_\infty V_\infty r_{SI}^{1+j} + \rho_w v_w r_w^{1+j} = \int_o^{\delta_{SI}} \rho u (2r)^j \, dy \tag{48}$$

At the wall, the boundary conditions for the boundary layer equations are the same as for the low Reynolds number viscous layer equations, and these are given by eqs. (36) to (38). The boundary conditions at the edge are as usual:

$$\lim_{y\to\infty} u(x, y) = u_e(x) \tag{49}$$

$$\lim_{y\to\infty} h(x, y) = h_e(x) \tag{50}$$

where $u_e(x)$ and $h_e(x)$ are determined from an inviscid solution as the values at the wall assuming no boundary layer. Since the boundary condition at the wall for the inviscid solution is

$$V_{w_{inv}} = 0 \tag{51}$$

then

$$h_e(x) = H_\infty - \frac{[u_e(x)]^2}{2} \tag{52}$$

In the stagnation region

$$u_e(x) \approx \frac{du_e}{dx} x \tag{53}$$

where the modified Newtonian velocity gradient is given by

$$\frac{du_e}{dx} = \frac{1}{R_B} \sqrt{\frac{2(p_e - p_\infty)}{\rho_e}} \tag{54}$$

Thus, for the boundary layer solutions we are assuming the inviscid flow is given by a modified Newtonian solution.

The boundary layer partial differential equations are of fifth order and the five boundary conditions are given by eqs. (36) to (38) and eqs. (49) and (50).

V. NORMALIZED SYSTEM OF EQUATIONS AND BOUNDARY CONDITIONS

In order to reduce the partial differential equations to ordinary differential equations, we employ a technique which has proven quite useful in treating the viscous layer (Refs. 2, 3, 21, 23, 24), namely an approximate separation of variables. The approximation involved is that terms of higher order in $K_B x$ than $K_B^2 x^2$ are being neglected. The variation in the x-direction is assumed to be given by a series compatible with the Rankine-Hugoniot relations, thereby yielding ordinary differential equations in y alone. The assumed form of the separation is the same as used in reference 3, i.e.,

$$u = K_B x\, u_1 (y) \tag{55}$$

$$v = \left(1 - \frac{1}{2} K_B^2 x^2\right) v_1 (y) \tag{56}$$

$$h = \left(1 - K_B^2 x^2\right) h_1 (y) - K_B^2 x^2\, h_2 (y) \tag{57}$$

$$\rho = \left(1 - \frac{1}{\gamma} K_B^2 x^2\right) \rho_1 (y) \tag{58}$$

$$p = \left(1 - K_B^2 x^2\right) p_1 (y) - K_B^2 x^2\, p_2 (y) \tag{59}$$

$$\mu = \left(1 - \frac{\gamma - 1}{2\gamma} K_B^2 x^2\right) \mu_1 (y) \tag{60}$$

$$r = x (1 + K_B y) \tag{61}$$

where the terms with subscripts 1 or 2 are functions of y alone. For convenience, the following non-dimensional forms are introduced:

$$\bar{u} = \frac{u_1}{V_\infty}\,,\quad \bar{V} = \frac{V_1}{\epsilon V_\infty}\,,\quad \bar{h}_1 = \frac{h_1}{V_\infty^2/2}\,,\quad \bar{h}_2 = \frac{h_2}{V_\infty^2/2}$$

$$\bar{\rho} = \epsilon \frac{\rho_1}{\rho_\infty}\,,\quad \bar{p}_1 = \frac{p_1}{\rho_\infty V_\infty^2}\,,\quad \bar{p}_2 = \frac{p_2}{\rho_\infty V_\infty^2} \tag{62}$$

$$\bar{\mu} = \frac{\mu_1}{\mu_s Re_s}\,,\quad \bar{y} = \frac{y}{R_B}$$

where the subscripts ∞ and s refer respectively to the free stream conditions and to a state immediately behind an equivalent normal shock wave given by

the Rankine-Hugoniot relations. In addition, a compressibility transformation is also introduced, i. e.

$$\eta = \int_0^{\bar{y}} \bar{\rho}\, d\bar{y} \tag{63}$$

With the above simplifications, the low Reynolds number viscous layer equations reduce to the following system of dimensionless non-linear ordinary differential equations with variable coefficients, to be used to obtain first order non-similar solutions in the forward region of a hypersonic vehicle:

$$(\bar{\rho}\bar{V})_\eta + (1+j)\left(\frac{\bar{u}}{\epsilon} + \bar{v}\right) = 0 \tag{64}$$

$$\bar{u}\left(\frac{\bar{u}}{\epsilon} + \bar{v}\right) + \bar{\rho}\bar{v}\bar{u}_\eta - 2\,\frac{\bar{p}_1 + \bar{p}_2}{\bar{\rho}} = (\bar{\rho}\bar{\mu}\bar{u}_\eta)_\eta + (2+j)\,\bar{\mu}\bar{u}_\eta - (\bar{\mu}\bar{u})_\eta \tag{65}$$

$$\epsilon\,\bar{\rho}\bar{v}\bar{v}_\eta + \bar{p}_{1_\eta} = \frac{4}{3}\,\epsilon\,(\bar{\rho}\bar{\mu}\bar{v}_\eta)_\eta + (1+j)\left[\bar{\mu}\bar{u}_\eta - \frac{2}{3}(\bar{\mu}\bar{u})_\eta\right] \tag{66}$$

$$\bar{p}_{2_\eta} + \bar{u}\left(\frac{\bar{u}}{\epsilon} + \bar{v}\right) = 0 \tag{67}$$

$$\bar{\rho}\bar{v}\bar{h}_{1_\eta} = \left(\frac{\bar{\rho}\bar{\mu}}{Pr}\,\bar{h}_{1_\eta}\right)_\eta + (1+j)\,\frac{\bar{\mu}}{Pr}\,\bar{h}_{1_\eta} \tag{68}$$

$$\bar{\rho}\bar{v}\bar{h}_{2_\eta} + 2\left[\left(\bar{\rho}\bar{\mu}\bar{u}\bar{u}_\eta\right)_\eta + (1+j)\,\bar{\mu}\bar{u}\bar{u}_\eta - (\bar{\mu}\bar{u}^2)_\eta\right]$$
$$= \left(\frac{\bar{\rho}\bar{\mu}}{Pr}\,\bar{h}_{2_\eta}\right)_\eta + (1+j)\,\frac{\bar{\mu}}{Pr}\,\bar{h}_{2_\eta} + 2\,\frac{\bar{u}}{\epsilon}\left[\bar{u}^2 + \epsilon\,\bar{\rho}\bar{V}\bar{u}_\eta - (\bar{h}_1 + \bar{h}_2)\right] \tag{69}$$

$$\bar{\rho} = \bar{\rho}\,(\bar{h}_1\,,\ \bar{p}_1) \tag{70}$$

$$\bar{\mu} = \bar{\mu}\,(\bar{h}_1\,,\ \bar{p}_1) \tag{71}$$

where the subscript η denotes derivatives with respect to η. It is seen that separation of the variables has increased the number of unknowns to eight,

including $\bar{u}$, $\bar{v}$, $\bar{h}_1$, $\bar{h}_2$, $\bar{p}_1$, $\bar{p}_2$, $\bar{\rho}$, $\bar{\mu}$. This requires that the number of governing equations also be eight, eqs. (64) to (71), while the overall order of the mathematical system is ten, requiring ten boundary conditions. The boundary conditions at the surface, $\eta = 0$, eqs. (36) to (38) become

$$\bar{u}_w = 0 \ , \ \bar{v}_w = \bar{v}_w$$

$$\bar{h}_{1_w} = \bar{h}_{1_w} = - \bar{h}_{2_w} \quad \text{(isoenthalpic wall)} \tag{72}$$

At the shock interface, $\eta = \eta_{SI}$ equations (44) through (47) become

$$(\bar{\rho}\bar{V})_{SI} = -1 \tag{73}$$

$$\bar{u}_{SI} = \frac{1 - \left(\bar{\rho}\bar{\mu}\bar{u}_\eta\right)_{SI}}{1 - \bar{\mu}_{SI}} \tag{74}$$

$$\bar{p}_{1_{SI}} = 1 - \epsilon - \frac{2}{3}\bar{\mu}_{SI}\left[(1+j)\,\bar{u}_{SI} - 2\epsilon\left(\bar{\rho}\bar{V}_\eta\right)_{SI}\right] \tag{75}$$

$$\bar{p}_{2_{SI}} = 0 \tag{76}$$

$$\bar{h}_{1_{SI}} = 1 - \epsilon^2 - \frac{\left(\bar{\rho}\bar{\mu}\bar{h}_{1_\eta}\right)_{SI}}{Pr} \tag{77}$$

$$\bar{h}_{2_{SI}} = - (1-\bar{u}_{SI})^2 - \frac{\left(\bar{\rho}\bar{\mu}\bar{h}_{2_\eta}\right)_{SI}}{Pr} \tag{78}$$

The constraint equation becomes:

$$(1 + \bar{\delta}_{SI})^{1+j} + \bar{\rho}_w \bar{v}_w = \int_0^{\bar{\delta}_{SI}} \frac{\bar{u}}{\epsilon}\left[2\,(1+\bar{y})\right]^j \, d\eta \tag{79}$$

Here it is noted that for the special case of zero mass transfer, i.e. $\bar{\rho}_w \bar{v}_w = 0$, examination of eq. (64) indicates that the constraint

$$\bar{v}'_w = 0 \tag{80}$$

becomes identical with eq. (79). This latter result (Ref. 2) follows from the fact that since $\bar{u}_w$ and $\bar{v}_w$ are both zero (for zero mass transfer), unless $\bar{v}_{\eta_w}$ also vanishes, one obtains the physically untenable result of an infinite density gradient at the wall, (Ref. 21).

The dimensionless boundary layer equations become

$$(\bar{\rho}\bar{v})_\eta + (1+j)\frac{\bar{u}}{\epsilon} = 0 \tag{81}$$

$$\left(\bar{\rho}\bar{\mu}\bar{u}_\eta\right)_\eta - \bar{\rho}\bar{v}\bar{u}_\eta + \frac{2}{\bar{\rho}} - \frac{\bar{u}^2}{\epsilon} = 0 \tag{82}$$

$$\left(\frac{\bar{\rho}\bar{\mu}}{Pr}\bar{h}_{l_\eta}\right)_\eta - \bar{\rho}\bar{v}\bar{h}_{l_\eta} = 0 \tag{83}$$

Note that the second energy equation is not included since it is usually assumed and our results, present and past (Ref. 3), indicate that the concept of similarity in the stagnation region at high Reynolds numbers is a good approximation. The boundary conditions at the surface ($\eta = 0$) are the same as eqs. (72), whereas at the edge of the boundary layer, eqs. (49) and (50) become

$$\lim_{\eta\to\infty} \bar{u}(\eta) = \bar{u}_e = \sqrt{2\epsilon} \tag{84}$$

$$\lim_{\eta\to\infty} \bar{h}(\eta) = \bar{h}_e = 1 \tag{85}$$

Here it is seen that this new formulation of the boundary layer equations and boundary conditions has the same form as that more commonly used (Refs. 1 and 17) and indeed the same asymptotic behavior at the edge.

In general, the transport properties depend on both temperature and composition. However, since the diffusion equations have been uncoupled, the composition of the gas is not calculated explicitly, and so it is necessary to resort to further approximations. Constant Prandtl and Lewis numbers

have already been introduced and hence the thermal conductivity and the diffusion coefficients are not required explicitly. Thus, only the viscosity coefficient remains to be evaluated.

It is assumed that the gas is in chemical equilibrium, or more explicitly that the state of the gas can be determined from a Mollier diagram (e. g. Ref. 33). That is, knowledge of two state functions (e. g. pressure and enthalpy) uniquely determines the others (e. g. temperature, composition, density, etc.). As already noted, it is assumed here that the viscosity coefficient can be approximated by Sutherland's formula for air (Ref. 34).

$$\mu = \mu\,(T) = 1.16 \times 10^{-5} \left(\frac{717}{225+T}\right)\left(\frac{T}{492}\right)^{3/2} \tag{86}$$

with T in ^{o}R, μ is given in lb_m/ft-sec. However, since (from the Mollier diagram)

$$T = T\,(h, p) \tag{87}$$

then implicitly

$$\mu = \mu\,(h, p) \tag{88}$$

and the equation of state may also be obtained from the Mollier diagram i. e.

$$\rho = \rho\,(h, p) \tag{89}$$

Conditions behind an equivalent normal shock were determined from shock tables which incorporate the 1959 ARDC model atmosphere, (Ref. 35).

VI. DISCUSSION OF RESULTS

Numerical solutions for both systems of equations with their appropriate boundary conditions were obtained on a high speed digital computer (IBM 7094). The range of hypersonic flight conditions for which calculations were obtained include flight velocities from 10,000 ft/sec. to 25,000 ft/sec.; altitudes from 100,000 ft. to 350,000 ft.; shock Reynolds numbers from 6 to 15,000; surface temperatures from 800°R to 3500°R; and dimensionless mass transfer rate parameter f_w from 0 to -0.4. The equations were integrated from the wall out to the shock interface for the low Reynolds number system and to the edge of the boundary layer for the other system. Since the boundary conditions are split, an iterative procedure was required.

Some typical solutions for the shock layer profiles of $\bar{u}$, $\bar{v}$, $\bar{h}$ and $\bar{p}$ are shown in figures 3 to 8. As expected, the viscous effects extend further into the shock layer with decreasing Reynolds number. Also, note the behavior of the flow variables at the shock interface with decreasing Reynolds number. Down to a shock Reynolds number of about 1000 the values are indistinguishable from those obtained with a discontinuous shock wave (Rankine-Hugoniot conditions) (Ref. 3), i.e., neglecting those terms in the boundary conditions (eqs. 73 to 78) containing the viscosity coefficient. Below a shock Reynolds number of 1000, merging of the two flow structures (shock wave and shock layer) is apparent, because the values of the flow variables at the shock interface are significantly different from that given by the Rankine-Hugoniot relations. That is, part of the shock layer structure is now merged and coupled with shock wave structure. In fact, upon examination of figure 5, where the shock Reynolds number is 1000, but including mass transfer, it is seen, that the normal component of velocity $\bar{v}$ is not that given by Rankine-Hugoniot considerations, thus indicating some merging at this Reynolds number. Also, note that although in figure 5 $\bar{v}_w$ appears to be zero the actual value is 0.0049, corresponding to $f_w = -0.4$. In figure 3, a comparison between a low

Reynolds number solution and a boundary layer solution at a shock Reynolds number of 15,000 is shown. It is seen, that even at this large a Reynolds number there is a significant deviation in the predicted profiles, especially in the tangential velocity component, $\bar{u}$, which shows up as a discrepancy in skin friction of thirty percent for this particular condition, while the enthalpy difference shows up as a ten percent difference in the heat transfer rate. It is readily seen that the difference in heat transfer is accountable for by the thinner viscous layer prediction of the low Reynolds number solution. However, quite vividly seen is that the major difference in skin friction is due to the raised level of the tangential velocity at the edge of the viscous layer, thus indicating that the boundary layer is not thin enough for boundary layer theory to be valid (i.e., edge conditions given by solution of the Euler equations at an inviscid wall).

Before discussing the low Reynolds number results, a comparison between the present boundary layer solutions (which are completely compatible with the present low Reynolds number solutions) and the precise boundary layer solutions obtained by Scala and Gilbert (Ref. 17), will be given. Scala and Gilbert utilized the now familiar hypersonic laminar boundary layer equations for a compressible viscous multicomponent chemically reacting gas, and the transport and thermodynamic properties were evaluated as a function of the local temperature and equilibrium gas composition. Preferential diffusion of the various gaseous species was included by evaluating the multicomponent Lewis numbers at surface conditions. The surface and outer boundary conditions were satisfied, assuming that the gas was in a state of thermochemical equilibrium throughout the boundary layer. They found that, in the absence of mass transfer, they could correlate all of their heat transfer results with

$$\left(C_{H_o}\sqrt{Re_s}\right)_{BL_{SG}} = \frac{V_\infty}{R_B\left(\frac{du_e}{dx}\right)_s} \tag{90}$$

and their skin friction results with

$$\left(\frac{2C_{H_o}}{C_{f_o}}\right)_{BL_{SG}} \left(\frac{X}{R_B}\right) = -0.35 + \left(C_H\sqrt{Re_s}\right)_{BL_{SG}} \tag{91}$$

where the Stanton number and skin friction coefficient are defined as

$$C_H = \frac{Q_w}{\rho_\infty V_\infty (H_s - h_w)} \tag{92}$$

$$\frac{C_f}{2} = \frac{\tau_w}{\rho_\infty V_\infty^2} \tag{93}$$

The subscript BL_{SG} refers to the boundary layer results of Scala and Gilbert, and the subscript o indicates the absence of mass transfer. Assuming a modified Newtonian velocity gradient (eq. 54), these correlations can be further reduced to

$$\left(C_{H_o}\sqrt{Re_s}\right)_{BL_{SG}} = \frac{1}{\sqrt{2\epsilon}} \tag{94}$$

$$\left(\frac{C_{f_o}}{2}\sqrt{Re_s}\right)_{BL_{SG}} = \frac{\sin(K_B x)}{1 - 0.35\sqrt{2\epsilon}} \tag{95}$$

The results of the present boundary layer solutions normalized with respect to those of reference (17) are summarized in figure 9. It is seen that the agreement is reasonable, i.e., since various previous boundary layer predictions also differ to about the same degree, see reference (28). In order to ascertain the reason for the discrepancies, new solutions were obtained with the present boundary layer formulation utilizing the density and viscosity variations obtained from Scala and Gilbert's solutions for the same flight conditions. With a Prandtl number of 0.71, no changes in the results were noted. However, when the Prandtl numbers were changed to those obtained by Scala and Gilbert the discrepancies were reduced to one half that shown in figure 9. This is quite surprising, since the differences in Prandtl number were no more than two or three percent. The remaining discrepancy is most likely due to neglecting preferential diffusion in the present model, i.e. a Lewis number of one was assumed in order to uncouple the diffusion equations.

In figure 10 the effects of air injected into air for the present boundary layer results are shown. These are in close agreement with those of reference (36). The dimensionless mass transfer parameter is defined as

$$B = \frac{\dot{m}_w (H_s - h_w)}{Q_{w_o}} \tag{96}$$

where $\dot{m}_w$ is the mass transfer rate related to the usual dimensionless mass transfer rate f_w as

$$f_w = \frac{-\dot{m}_w}{\sqrt{(1+j)\,\rho_w \mu_w \left(\frac{du_e}{dx}\right)_s}} \tag{97}$$

Note, the slopes $\partial Q_w / \partial \dot{m}_w$ and $\partial \tau_w / \partial \dot{m}_w$ are not constants.

The normalized heat transfer rates can be seen in figure 11 over a very wide range of Reynolds numbers. The abscissa $\epsilon^2 Re_s$ was first used in reference 3 in order to correlate the viscous layer heat transfer results (outer boundary conditions given by the Rankine-Hugoniot relations); these results are also shown in figure 11. The present results are seen to have a Mach number dependence when merging occurs. (More results have been obtained but have been omitted for clarity; the trends are the same.) Included in this figure are the results of Cheng (Refs. 25 and 32), in whose analysis the governing equations do not contain the higher order (Re_s^{-1}) terms, and the results of Kao (Ref. 26) who was required to utilize three different theories (i.e., second and third order boundary layer theories plus, at the lowest Reynolds numbers, integration through the shock) in order to cover the low Reynolds number regime. It is also seen that the present results extend, by about one order of magnitude, to lower values of $\epsilon^2 Re_s$, than the aforementioned studies, primarily due to the orbital hypersonic values of ϵ used in the present study. These lower values of ϵ are seen to raise the predicted heat transfer rates in excess of fifty percent above boundary layer predictions, and can, thus, not be reasonably neglected.

To see if these Mach number effects were noticeable at even lower Reynolds numbers, i.e., out in the near free molecule and free molecule regimes, earlier results of Willis (Ref. 11) in the near free molecule regime, correlated by Hamel (Ref. 37), which showed very little Mach number effect as a function of free stream Reynolds numbers, were re-examined as a function of the parameter $\epsilon^2 Re_s$ and are also shown in figure 11. Note

$$Re_s = \frac{\mu_\infty}{\mu_s} Re_\infty \tag{98}$$

and μ_s is evaluated from Rankine-Hugoniot considerations. The same relative Mach number trend is also seen at these very low Reynolds numbers.

Even though any of the other merged layer results could just as reasonably be interpolated between their results and the modified Willis results, only the

present results have been so extended, and the interpolations are shown as dashed curves. In all of these studies, all of the accommodation coefficients have been assumed to be unity.

The assumption of local similarity appears to break down at lower Reynolds numbers in contradiction to the conclusions of Kao (Ref. 38). Note that at the particular low Reynolds number ($Re_s = 10$) where Kao tested the similarity concept, similarity appears to be reasonable. However, this is clearly a coincidence. Therefore, his conclusion concerning the validity of local similarity over the entire range of Reynolds number does not seem to be correct. Note the two components of the heat transfer rate are combined as

$$Q_w = Q_{w_1} \cos^2 (K_B x) + Q_{w_2} \sin^2 (K_B x) \tag{99}$$

to yield the heat transfer rate around the forward region of the body. The present non-similar correlations are uniformly valid out to angles as large as

$$\sin^2 (K_B x)_{MAX} = 0 (\epsilon) \tag{100}$$

and are for an isoenthalpic surface.

Another interesting point to be seen from the results of figure 11 is that the low Reynolds number effects appear to decrease with increasing shock density ratio ϵ. This seems to be a reasonable trend since, as noted earlier,

$$\delta_s = 0 (\epsilon R_B) \tag{101}$$

Therefore, the boundary layer thickness, δ_{BL} which varies as

$$\delta_{BL} \propto \frac{1}{\sqrt{Re_s}} \tag{102}$$

can increase more, for larger ϵ, before becoming significant with respect to δ_s. On the other hand, the shock wave thickness Δ_s varying as

$$\Delta_s \propto \frac{1}{Re_s} \tag{103}$$

continues to increase and takes over, decreasing the trends before the other

low Reynolds number effects become significant. This would appear to clear up some of the discrepancies in the reported low Reynolds number effects (Refs. 2, 3, 18-26, 32, 39, 40). Again it is stressed that the real gas orbital hypersonic density ratios show significant low Reynolds number effects.

Another possible cause of the discrepancies was indicated in reference 3. There it was shown that the only other study that had carefully obtained a boundary layer asymptote consistent with the low Reynolds number study (Ref. 22) (both theoretically and experimentally), had an almost identical correlation for heat transfer to that obtained in reference 3.

Even more significant low Reynolds number effects can be seen in figure 12 which shows the normalized skin friction as a function of $\epsilon^3 Re_s$. The same Mach number dependence is seen, however, greatly amplified. Again included are the results of Kao for purposes of comparison. Here it is seen that consideration of the low Reynolds effects can be all important for maneuvering or very slender ballistic re-entry vehicles. Again the same Mach number effects are seen in the near free molecule regime. The interpolations are again shown by dashed curves. Note that at the highest Reynolds numbers computed, $Re_s = 15,000$, the first component of the heat transfer rate and the skin friction predictions are ten and thirty percent respectively, above boundary layer theory predictions, indicating the strong effects of the vorticity in the inviscid flow, or equivalently, the boundary layer is not yet "thin" with respect to the shock layer thickness. The curves are extrapolated to the high Reynolds numbers asymptote.

The effect of mass transfer of air on the heat transfer rate in the low Reynolds number regime is also shown in figure 10. However, in the definition of B, eq. (96), Q_{w_o} is now the low Reynolds number value of the heat transfer rate in the absence of mass transfer for the same flight conditions. The single curve represented all the mass transfer results except at the lowest Reynolds numbers, i. e.

$$Re_s \leq 0(30) \tag{104}$$

where the results rapidly climbed above the curve. However, the validity of

the present model itself becomes questionable at these low Reynolds numbers and even more so in the presence of relatively large mass transfer rates.

Interestingly, the zero mass transfer skin friction results in figure 12 are also the correlations in the presence of mass transfer. Again, at the lowest Reynolds numbers, i.e.,

$$Re_s \leq 0\,(40) \tag{105}$$

the results are above the curve.

Although considerations of the tangential transport of mass in the shock wave are important for determining the location of the shock interface and other aspects of the shock layer structure, the maximum effect on the skin friction and the heat transfer rate is insignificant, i.e., less than four percent and one percent respectively, even at the lowest Reynolds numbers considered.

A further indication of the lower limit of validity of the present analysis is shown in figure 13, where the present correlation of the first component of pressure is compared with the experimental curve-fitted data of Potter and Bailey (Ref. 41) for hemispherical-nosed probes in Nitrogen. The agreement is excellent (within one percent) for

$$\frac{Re_s}{\sqrt{\epsilon}} \geq 200 \tag{106}$$

or

$$Re_s \geq 0\,(50) \tag{107}$$

in agreement with the mass transfer limitations, eqs. (104) and (105).

It has been suggested (Ref. 42) that the actual (experimental) behavior of $p_{l_w}/p_{stag_{BL}}$ may be explained as follows: At very high Reynolds numbers (very thin boundary layer) the flow behind the shock is brought isentropically to rest. As the Reynolds number decreases (viscous effects extend further into the shock layer) viscous losses occur and the actual stagnation pressure is less than the isentropic prediction. With further rarefaction, the shock thickens such that it begins to lose its continuum character and approaches a

molecular model. Eventually, the shock wave thickens sufficiently to include the entire flow field, the rarefaction effects predominate over the viscous effects and the pressure increases. With sufficient rarefaction more of the molecules make a more direct impact on the body as the free molecule limit is approached. It is clear that a strictly continuum analysis cannot account for all of the foregoing processes; therefore the divergence of the results when eq. (106) is violated.

Re-examining figures 11 and 12, it is seen that eq. (106) suggests that the lower limitation of the present theoretical study is slightly to the left of the peaks in $Q_{w_o}/Q_{w_{o_{BL}}}$ (figure 11) and slightly to right of the peaks in $\tau_w/\tau_{w_{BL}}$ (figure 12). The viscous layer prediction of the variation of $\overline{p}_l$ (Ref. 3), although not correlated by the same parameter, shows only an increasing $\overline{p}_l$ with decreasing Reynolds number. Furthermore, it is seen that the viscous layer predictions of heat transfer rates and skin friction are greater than the merged layer results. Thus, in the light of figure 13, plus the results of reference 3, it might seem as though peaks might be broader to the left for heat transfer and even possibly higher and broader to the left for skin friction. In order to assess this jump condition, new solutions were obtained in an ad-hoc manner by replacing the theoretical boundary condition $p_{l_{SI}}$ given by eq. (75) with p_{l_W} determined from the experimental results of reference 41. Even at the lowest Reynolds numbers considered ($Re_s = 10$), the heat transfer rate predictions were virtually unchanged while those of the skin friction were less than five percent above that given in figure 12. Since other wall slip effects are probably also of importance at these low Reynolds numbers, all should be included in a consistent manner to assess this effect properly. However, without further study of surface slip effects, the results as presented in figures 11 and 12 are believed to be the best available at present.

The abscissa, $Re_s/\sqrt{\epsilon}$, used to very effectively correlate p_l, was derived in reference 41 from viscous layer and Rankine-Hugoniot considerations.

The correlations for the second component of pressure are shown in figure 14. Following eq. (59) the two components are combined as follows

$$p_w = p_{1_w} \cos^2 (K_B x) - P_{2_w} \sin^2 (K_B x) \qquad (108)$$

to yield the pressure at the surface around the forward region of the body. Note that p_2, which accounts for centrifugal effects, is disappearing with decreasing Reynolds numbers, a further indication of a break down of the continuum character of the flow.

VII. CONCLUSIONS

1. Non-similar heat transfer rates, skin friction and normal surface pressures have been correlated from the lowest limit ($Re_s = 0\ (50)$) of the present model up to the high Reynolds number boundary layer asymptote.

2. In order to compare results in the low Reynolds number regime with those from boundary layer theory one must use a compatible boundary layer analysis.

3. The low Reynolds number effects, obtained in this study, are due to a combination of several effects. These include: a thinner viscous layer than predicted by boundary layer theory, vorticity in the "inviscid" region of the flow field, and a larger region for the flow parameters to change from free stream values to surface conditions when merging occurs.

4. The effects of hypersonic normal shock density ratios ($\epsilon \leq 0(0.1)$) are noted by larger heat transfer rates and skin friction with decreasing ϵ, in the low Reynolds number regime.

5. The benefits obtained with mass transfer in the high Reynolds number regime (i.e. reduction of heat transfer rates and skin friction) have been shown to extend into the low Reynolds number regime.

6. The implications of the present analysis can be very important for various applications. An example would be the increased heat transfer rate predictions on very small particles that have penetrated into the atmosphere and are still at low Reynolds numbers when experiencing maximum heating rates. On the other hand, for large manned re-entry vehicles which must maneuver and decelerate at high altitudes, one must have adequate knowledge of the forces and moments at low Reynolds numbers.

VIII. REFERENCES

1. Hayes, W. D. and Probstein, R. F., "Hypersonic Flow Theory", Academic Press, New York, 1959.

2. Goldberg, L. and Scala, S. M., "Mass Transfer in the Hypersonic Low Reynolds Number Viscous Layer", IAS Preprint 62-80, Presented at the IAS Thirtieth Annual Meeting, New York City, January 22, 1962.

3. Goldberg, L. and Scala, S. M., "Mass Transfer in the Low Reynolds Number Viscous Layer Around the Forward Region of a Hypersonic Vehicle", General Electric Company, MSD, TIS R65SD27, 1965.

4. Gilbert, L. M. and Scala, S. M., "Free Molecular Heat Transfer in the Ionosphere", AAS Preprint 61-72 to appear in the Proceedings of the American Astronautical Society Symposium on Interactions of Space Vehicles with an Ionized Atmosphere, Washington, D. C., 1961.

5. Wachman, H. Y., "The Effect of Surface Properties on Energy Transfer at Low Gas Densities", Proceedings of General Electric Co., MSVD, High Altitude Aerodynamics Conference, Paper 2.3, 1961.

6. Wachman, H. Y., "Thermal Accommodation Coefficient: A Critical Survey", ARS Journal, Vol. 32, No. 1, p. 1, 1962.

7. Hartnett, J. P., "A Survey of Thermal Accommodation Coefficients", Proceedings of the Second Rarefied Gas Dynamics Symposium, Academic Press, pp. 1-28, 1960.

8. Willis, D. R., "A Study of Some Nearly Free Molecular Flow Problems", Ph. D. dissertation, Princeton University, Princeton, New Jersey, 1958.

9. Baker, R. M. L., Jr. and Charwat, A. F., "Transitional Correction to the Drag of a Sphere in Free Molecule Flow", Phys. Fluids, Vol. 1, pp. 73-81, 1958.

10. Enoch, J., "A Kinetic Model for Hypersonic Rarefied Gas Flow", General Electric Co., MSVD, TIS R61SD063, 1961.

11. Willis, D. R., "Methods of Analysis of Nearly Free Molecule Flow For a Satellite or Other Space Vehicle", General Electric Co., MSVD, TIS R60SD399.

12. Hamel, B. B., "A Model for the Transition Regime in Hypersonic Rarefied Gas Dynamics", AIAA Journal, Vol. 2, No. 6, June 1964.

13. Prandtl, L., "Über Flüssigkeitsbewegung bei sehr kleiner Reibung", Proceedings of the III International Math Congress, Heidelberg, 1904.

14. Lees, L., "Laminar Heat Transfer Over Blunt Bodies at Hypersonic Flight Speeds", Jet Propulsion, Vol. 26, pp. 259-269, 1956.

15. Fay, J. A. and Riddell, F. R., "Theory of Stagnation Point Heat Transfer in Dissociated Air", J. Aero. Sci., Vol. 25, pp. 78-85, 1958.

16. Scala, S. M., "A Study of Hypersonic Ablation", Proceedings of the Tenth International Astronautical Federation Congress, London, Springer Verlag, pp. 790-828, 1959.

17. Scala, S. M. and Gilbert, L. M., "Theory of Hypersonic Laminar Stagnation Region Heat Transfer in Dissociating Gases", General Electric Co., MSD, TIS R63SD40, April 1963. Developments in Mechanics (Ed. S. Ostrach), Pergamon Press, pp. 643-683, 1965.

18. Hoshizaki, H., "Shock-Generated Vorticity Effects at Low Reynolds Numbers", Lockheed Missiles and Space Division, LMSD 48481, Vol. 1, pp. 9-43, Jan. 1959.

19. Oguchi, H., "Blunt Body Viscous Layer With and Without a Magnetic Field", Phys. of Fluids, Vol. 3, pp. 567-580, 1960.

20. Hoshizaki, H., Neice, S. and Chan, K. K., "Stagnation Point Heat Transfer Rates at Low Reynolds Numbers", IAS Preprint 60-68, Presented at IAS Nat. Sum. Meet., June 28-July 1, 1960.

21. Ho, H. T. and Probstein, R. F., "The Compressible Viscous Layer in Rarefied Hypersonic Flow", Brown University, ARL TN 60-132, Aug. 1960. Also published in Proceedings of the Second Rarefied Gas Dynamics Symposium, Academic Press, pp. 525-552, 1960.

22. Ferri, A., Zakkay, V. and Ting, L., "Blunt Body Heat Transfer at Hypersonic Speeds and Low Reynolds Numbers", J. Aero. Sci., Vol. 28, pp. 962-971, 1961.

23. Probstein, R. F. and Kemp. N. H., "Viscous Aerodynamic Characteristics in Hypersonic Rarefied Gas Flow", J. Aero. Sci., Vol. 27, pp. 174-192, 218, 1960.

24. Levinsky, E. S. and Yoshihara, H., "Rarefied Hypersonic Flow Over a Sphere", Presented at the ARS International Hypersonics Conference, MIT, Cambridge, Massachusetts, 1961.

25. Cheng, H. K., "Hypersonic Shock-Layer Theory of the Stagnation Region at Low Reynolds Number", Proceedings of the 1961 Heat Transfer and Fluid Mechanics Institute, Stanford University Press, Stanford, California, 1962.

26. Kao, H. C., "Hypersonic Viscous Flow Near the Stagnation Streamline of a Blunt Body: II. Third-Order Boundary-Layer Theory and Comparison with Other Methods", AIAA Jour., Vol. 2, pp. 1897-1906, 1964.

27. Li, T. Y. and Geiger, R. E., "Stagnation Point of a Blunt Body in Hypersonic Flow", J. Aero. Sci., Vol. 24, pp. 25-32, 1957.

28. Scala, S. M. and Baulknight, C. W., "Transport and Thermodynamic Properties in a Hypersonic Laminar Boundary Layer: Part 2, Applications", ARS Journal, Vol. 30, No. 4, pp. 329-336, 1960.

29. Sedov, L. I., Michailova, M. P. and Chernyi, G. G., "On the Influence of Viscosity and Heat Conduction on the Gas Flow Behind a Strong Shock Wave", Vestnik Moskovskovo Unversiteta, No. 3, p. 95, 1953.

30. Probstein, R. F. and Pan, Y. S., "Shock Structure and the Leading Edge Problem", Rarefied Gas Dynamics, Vol. II (ed. by J. A. Laurmann), Academic Press, New York, 1963.

31. Pan, Y. S. and Probstein, R. F., "Rarefied Flow Transition at a Leading Edge", MIT, Fluid Mechanics Lab. Publication No. 64-8, 1964.

32. Cheng, H. K., "The Blunt-Body Problem in Hypersonic Flow at Low Reynolds Number", Cornell Aeronautical Laboratory, CAL Report No. AF-1285-A-10, June, 1963.

33. Moeckel, W. E. and Weston, K. C., "Composition and Thermodynamic Properties of Air in Chemical Equilibrium", NACA TN 4265, 1958.

34. Jeans, J. H., "The Dynamical Theory of Gases", Dover Publications, Inc., New York, 1954.

35. Cook, C. A., Gilbert, L. M. and Scala, S. M., "Normal Shock Wave Calculations in Air at Flight Speeds Up to 25,000 Ft./Sec.", General Electric Company, MSD, TIS R62SD76, November 1962.

36. Scala, S. M., "Transpiration Cooling in the Hypersonic Laminar Boundary Layer", General Electric Co., MSVD, TIS 58SD215, March 1958.

37. Hamel, B. B., Private Communication.

38. Kao, H. C., "Hypersonic Viscous Flow Near the Stagnation Streamline of a Blunt Body: I. A Test of Local Similarity", AIAA Jour., Vol. 2, pp. 1892-1897, 1964.

39. Vidal, R. J. and Wittliff, C. E., "Hypersonic Low Density Studies of Blunt and Slender Bodies", Rarefied Gas Dynamics, Vol. II, (Ed. by J. A. Laurmann), Academic Press, New York, pp. 343-378, 1963.

40. Hacker, D. S. and Wilson, L. N., "Shock Tube Results for Hypersonic Stagnation Heating at Very Low Reynolds Numbers", Proceedings of the Symposium on Dynamics of Manned Lifting Planetary Entry, (Eds. Scala, Harrison and Rogers), Oct. 1962, John Wiley and Sons, Inc., New York, 1963.

41. Potter, J. L. and Bailey, A. B., "Pressures in the Stagnation Regions of Blunt Bodies in the Viscous-Layer to Merged-Layer Regimes of Rarefied Flow", AIAA Preprint 63-436, Presented at the AIAA Conference of Physics of Entry into Planetary Atmospheres, at MIT, August 26-28, 1963.

42. Daum, F. L., Shang, J. S. and Elliott, G. A., "Impact-Pressure Behavior in Rarefied Hypersonic Flow", Office of Aerosapce Research, Research Review, Vol. IV, No. 2, April, 1965.

Acknowledgments

The author is pleased to acknowledge the assistance of the scientific programming staff of the Theoretical Fluid Physics Section. In particular Messers. Frank Bosworth and James Massey for programming the Low Reynolds number equations and Stephen Schechner for programming the boundary layer equations.

The analysis is based on work which was supported by the National Aeronautics and Space Administration, Space Nuclear Propulsion Office contract SNPC-29.

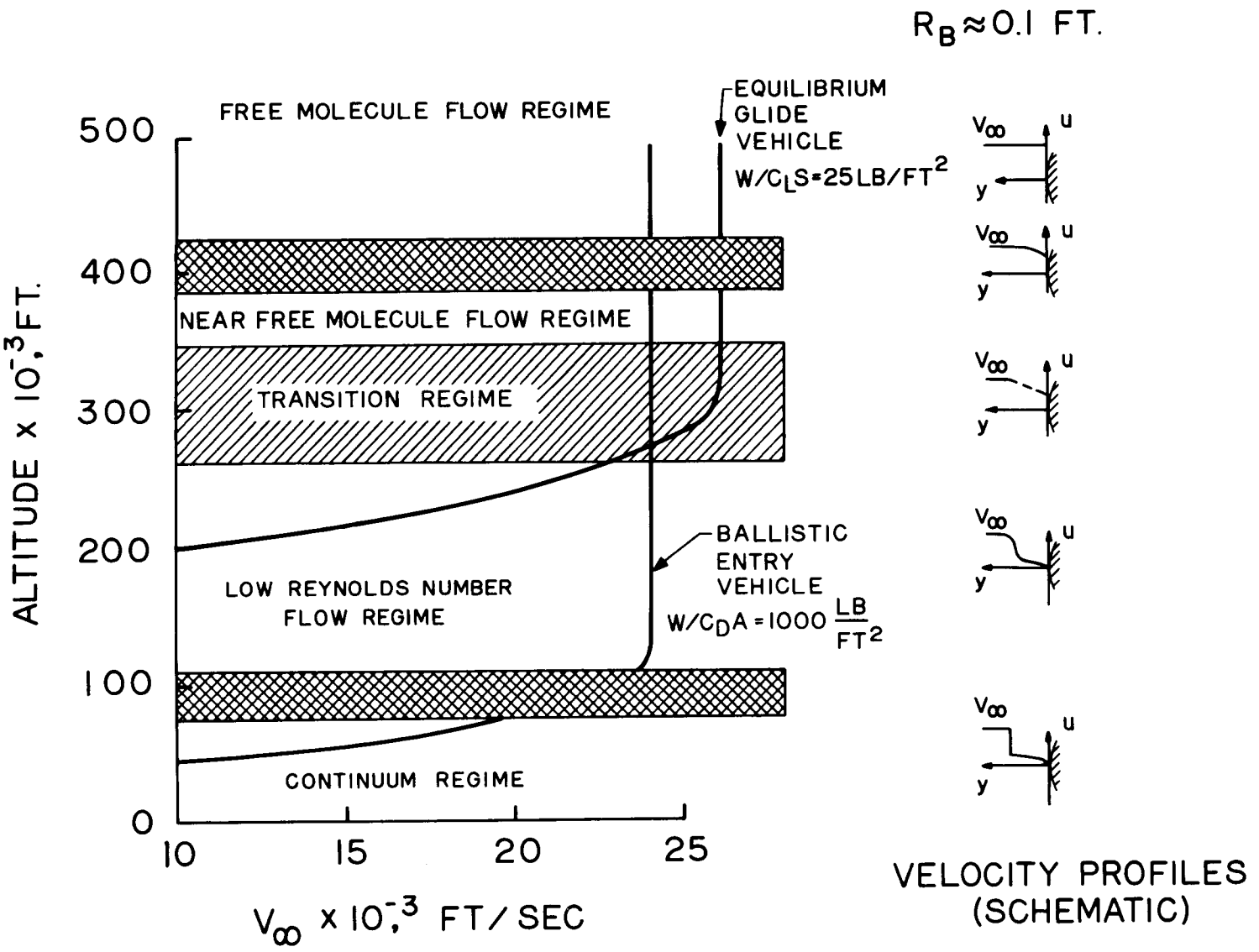

Figure 1. Hypersonic Flight Regimes

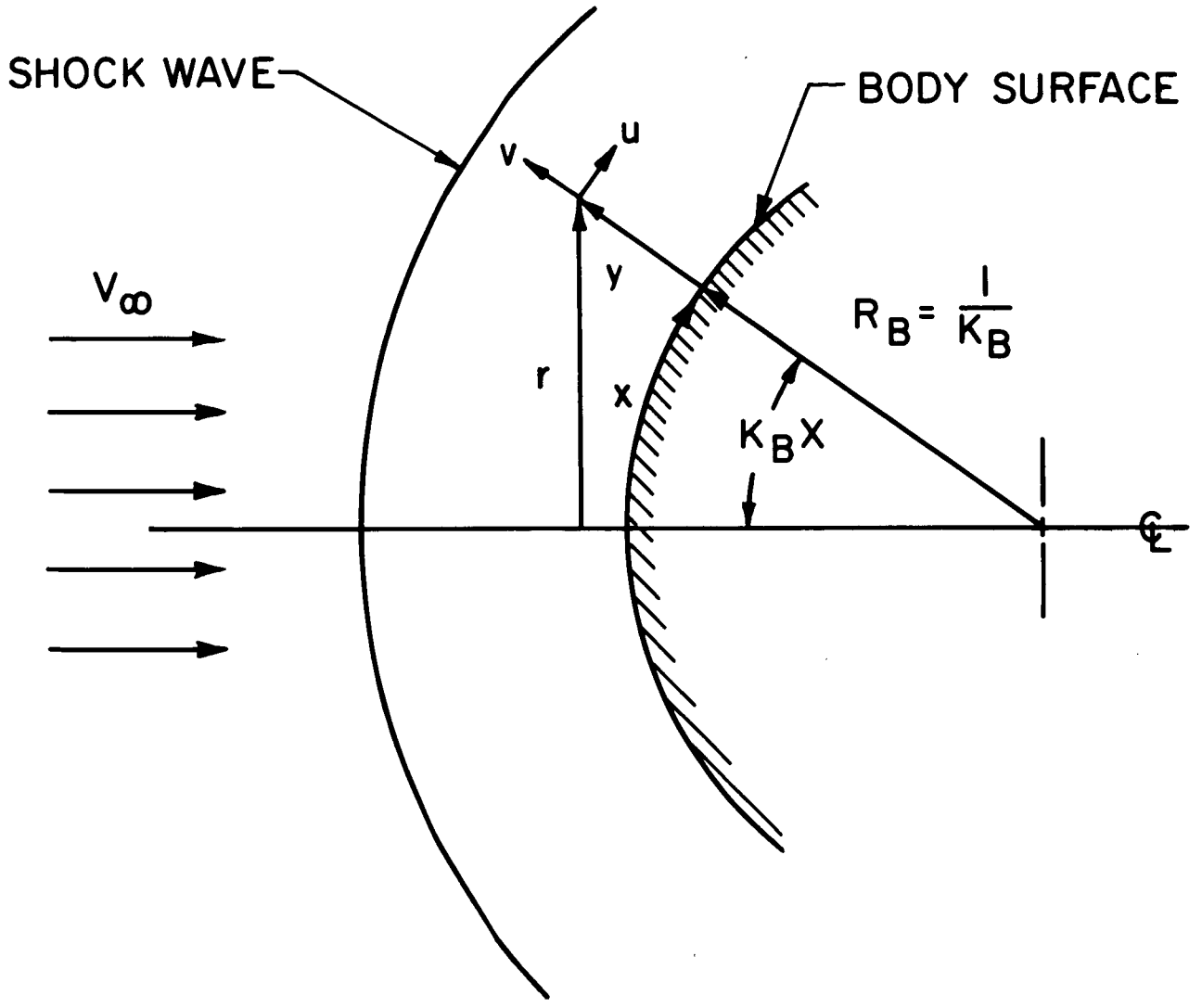

Figure 2. Coordinate System

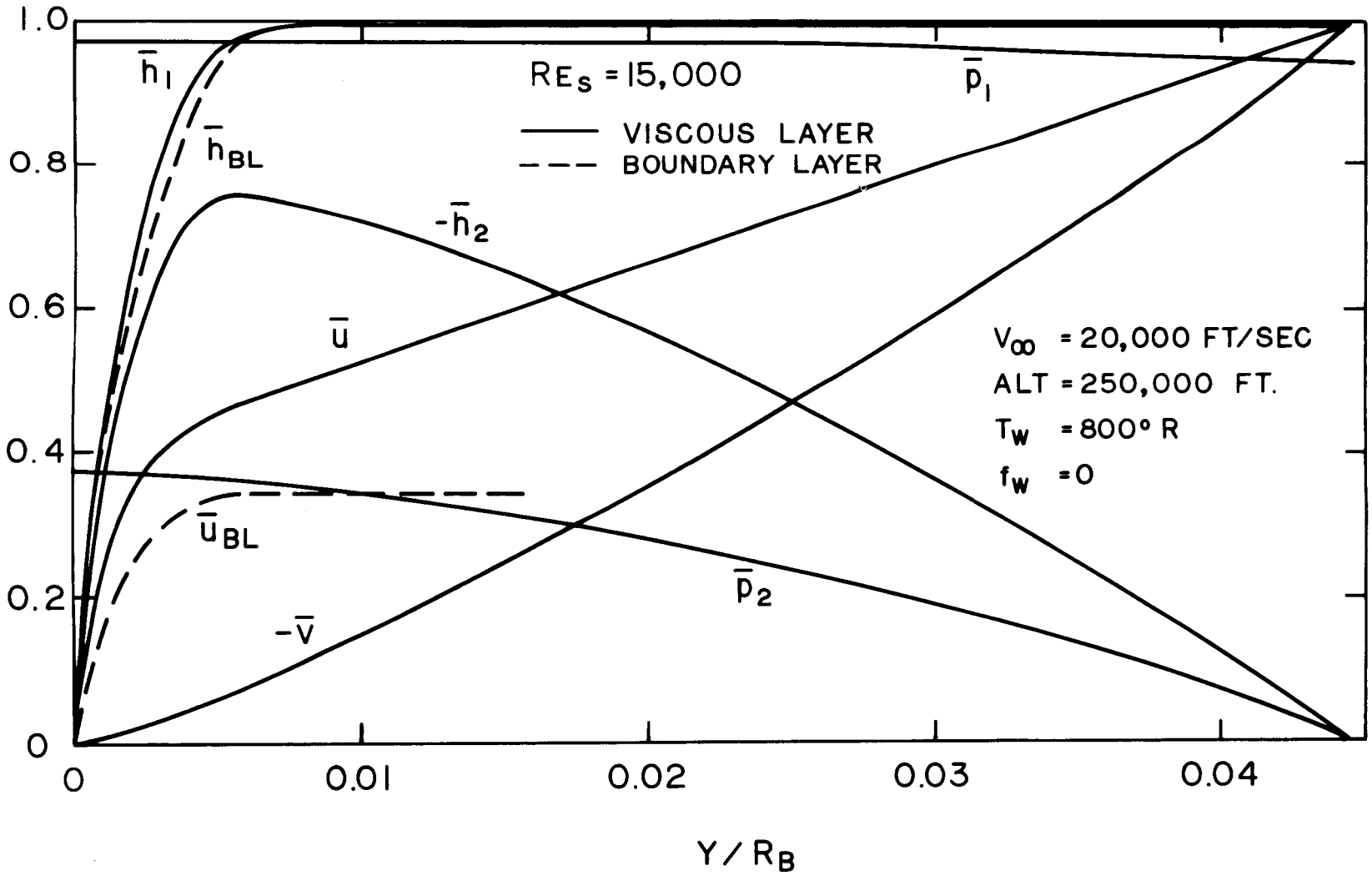

Figure 3. Comparison between a merged viscous layer solution and a boundary layer solution in the forward region of a sphere at Re_s = 15,000

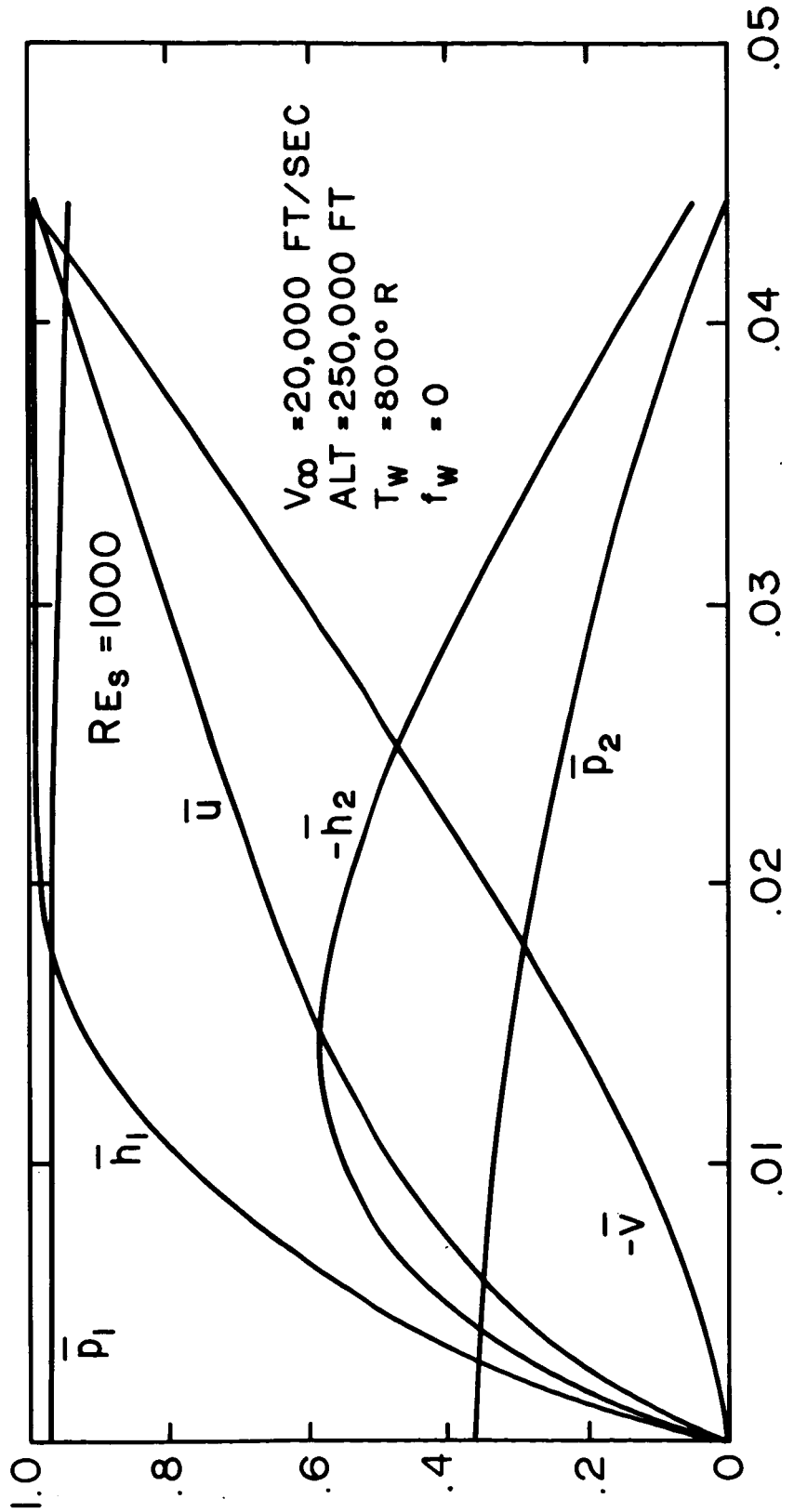

Figure 4. Profiles $Re_s = 10^3$

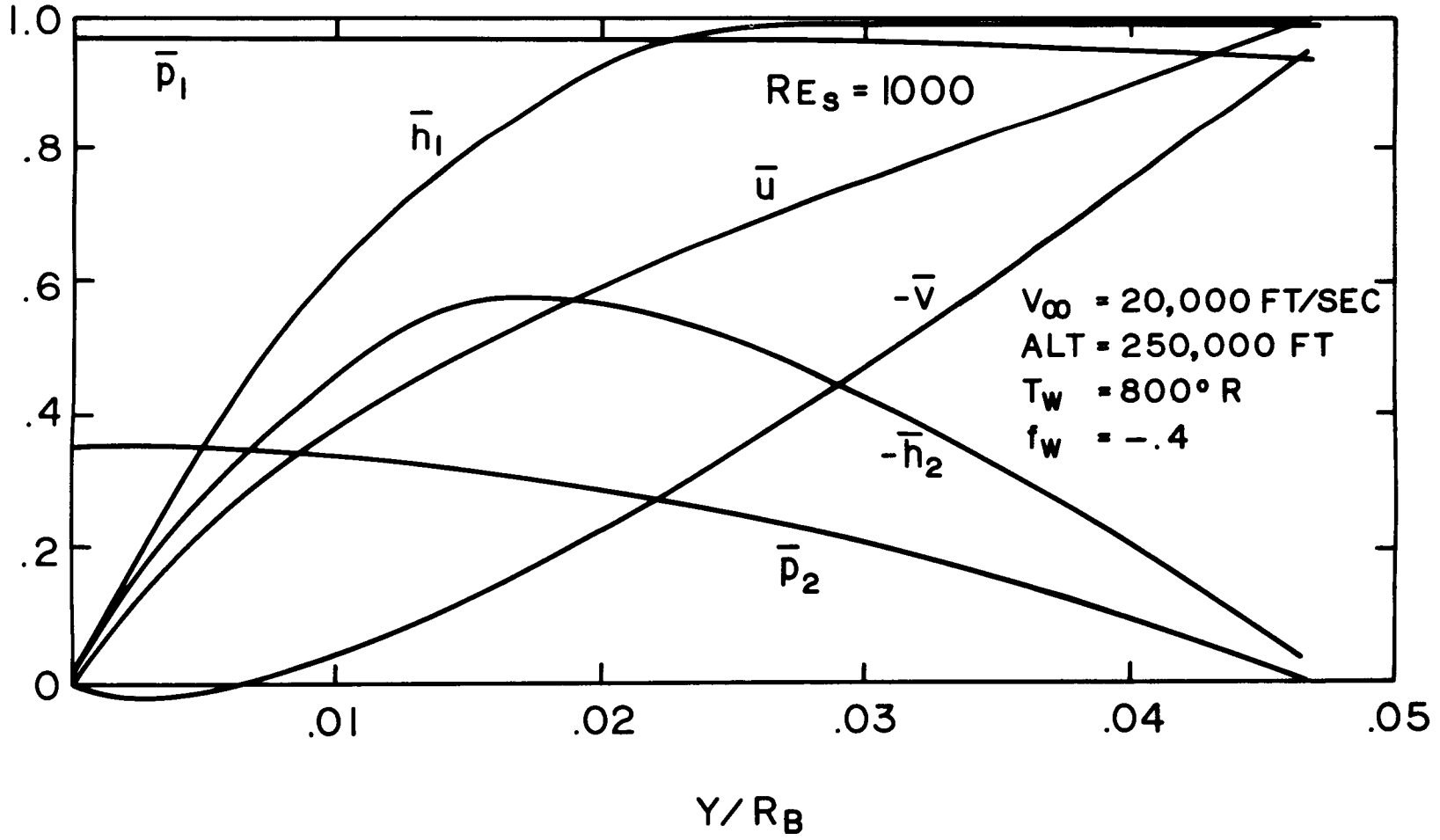

Figure 5. Profiles $Re_s = 10^3$, $f_w = -0.4$

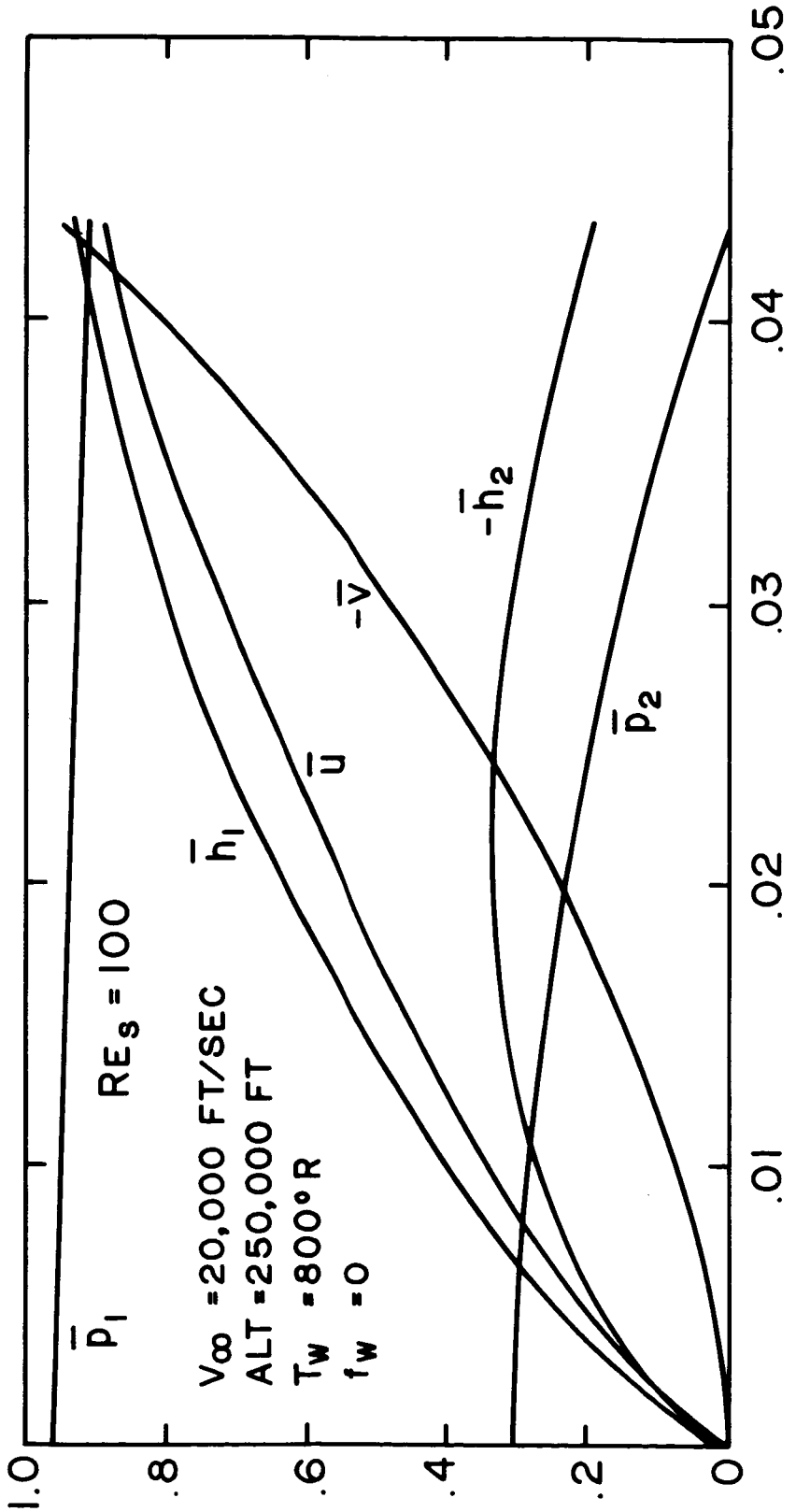

Figure 6. Profiles $Re_s = 10^2$

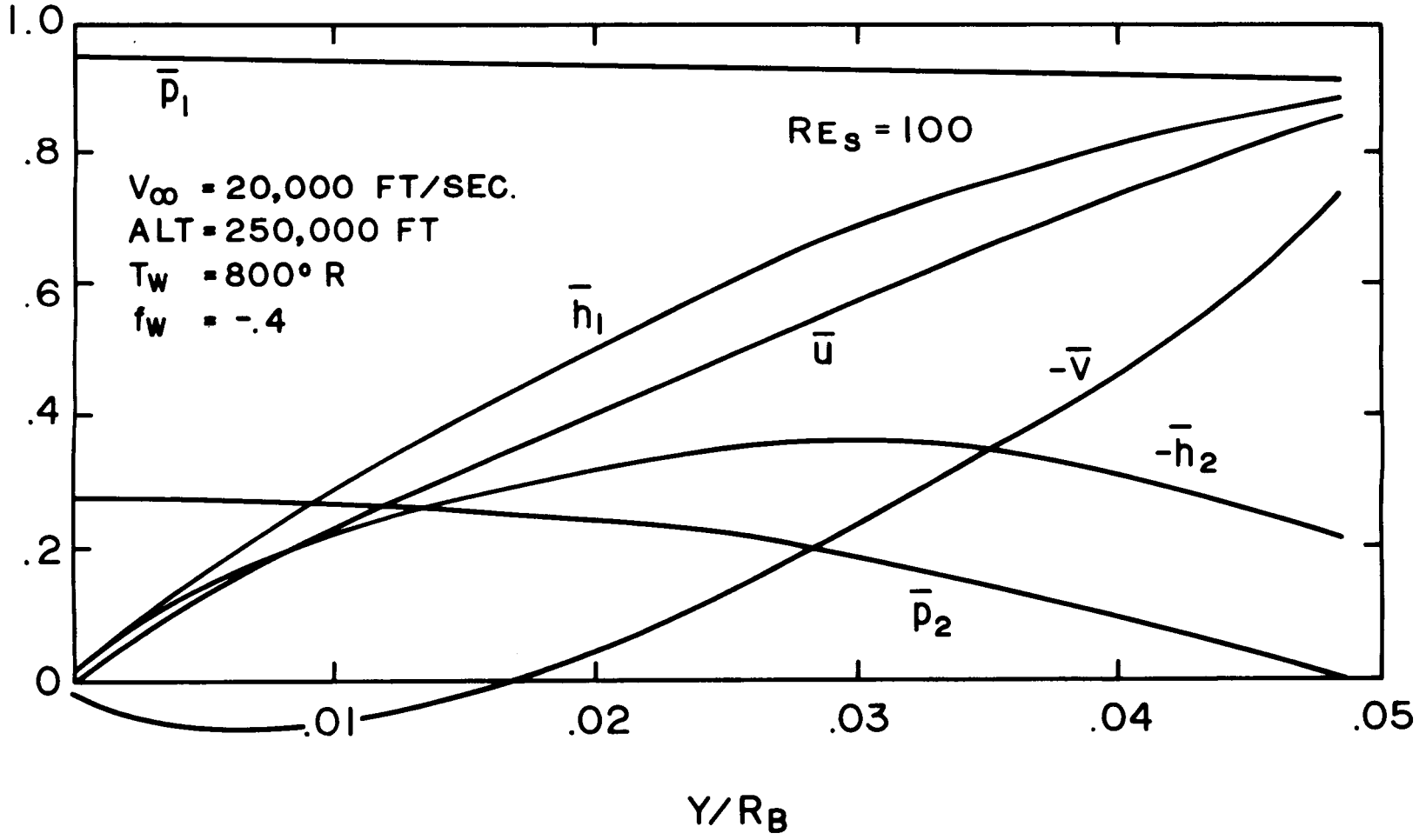

Figure 7. Profiles $Re_s = 10^2$, $f_w = -0.4$

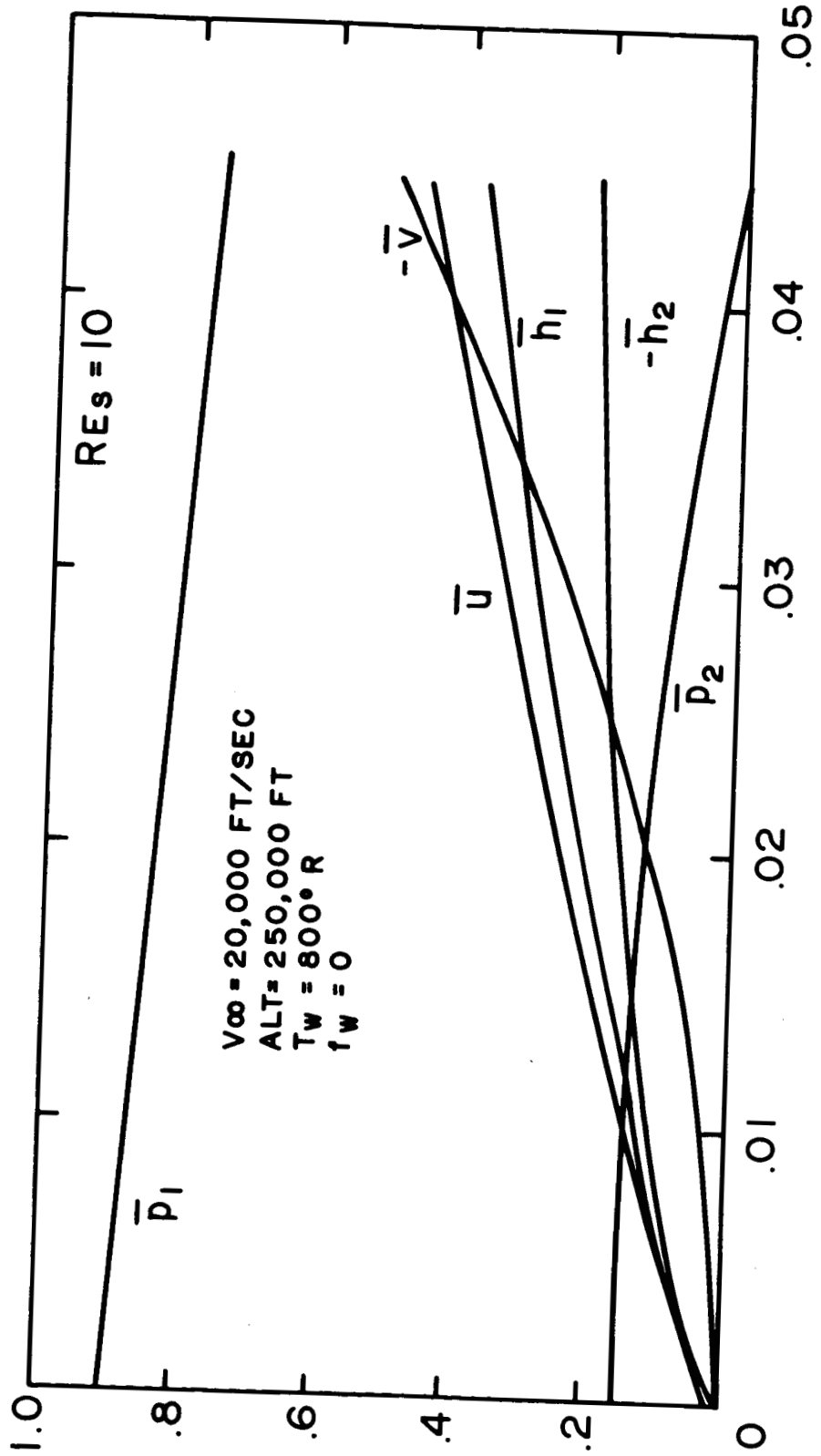

Figure 8. Profiles $Re_s = 10$

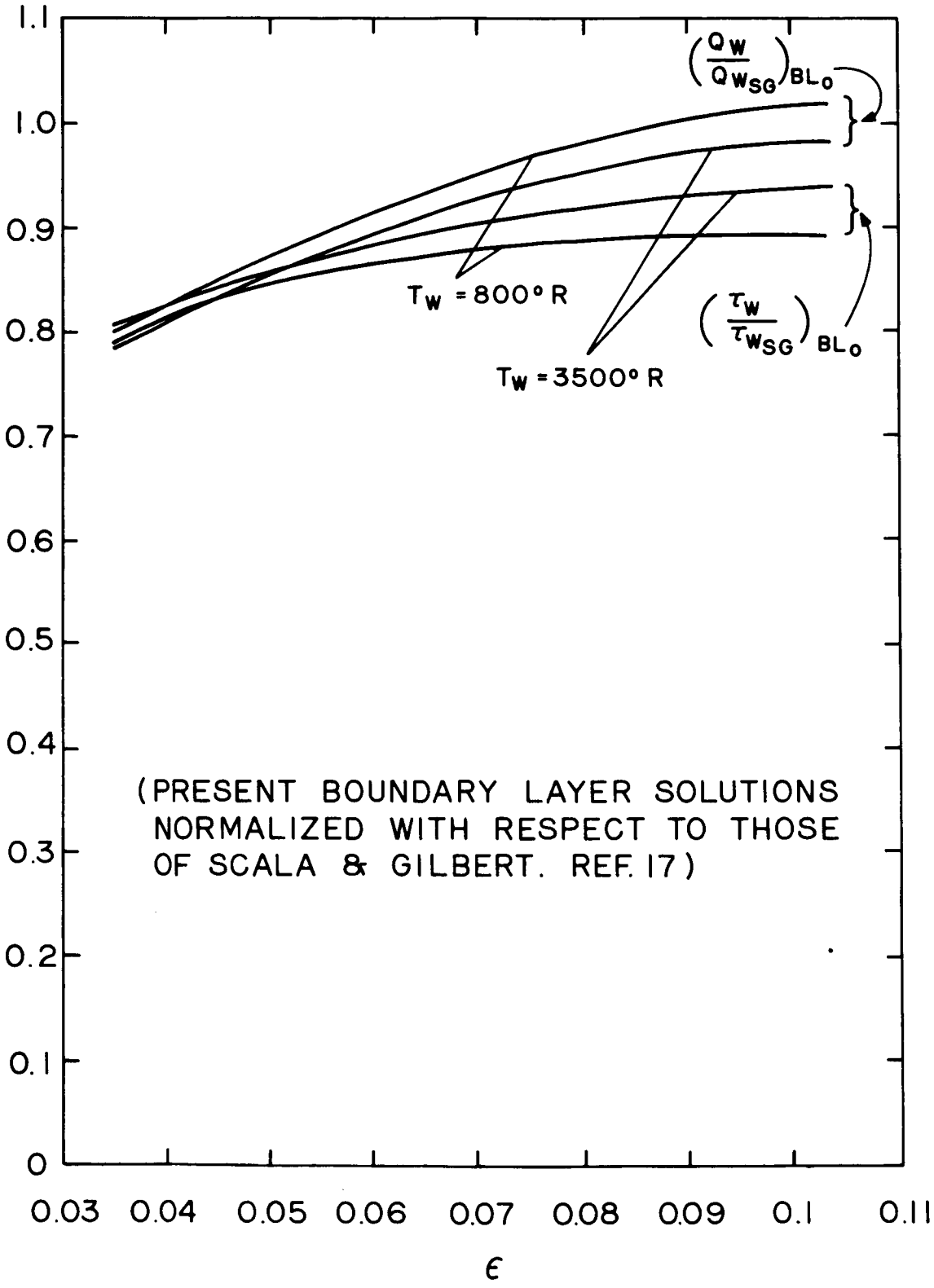

Figure 9. Normalized Boundary Layer Correlations

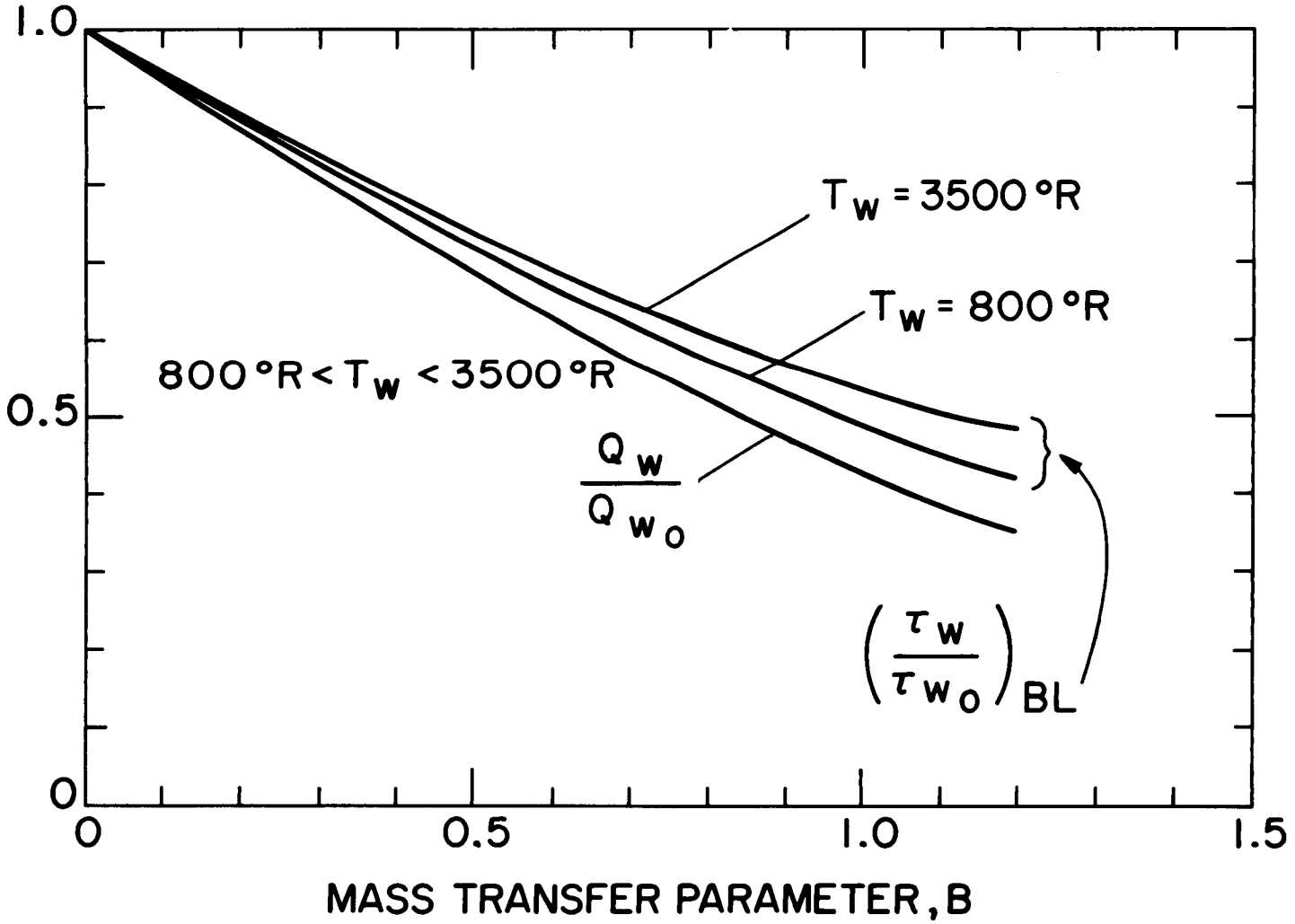

Figure 10. Effects of Mass Transfer on Heat Transfer and Skin Friction

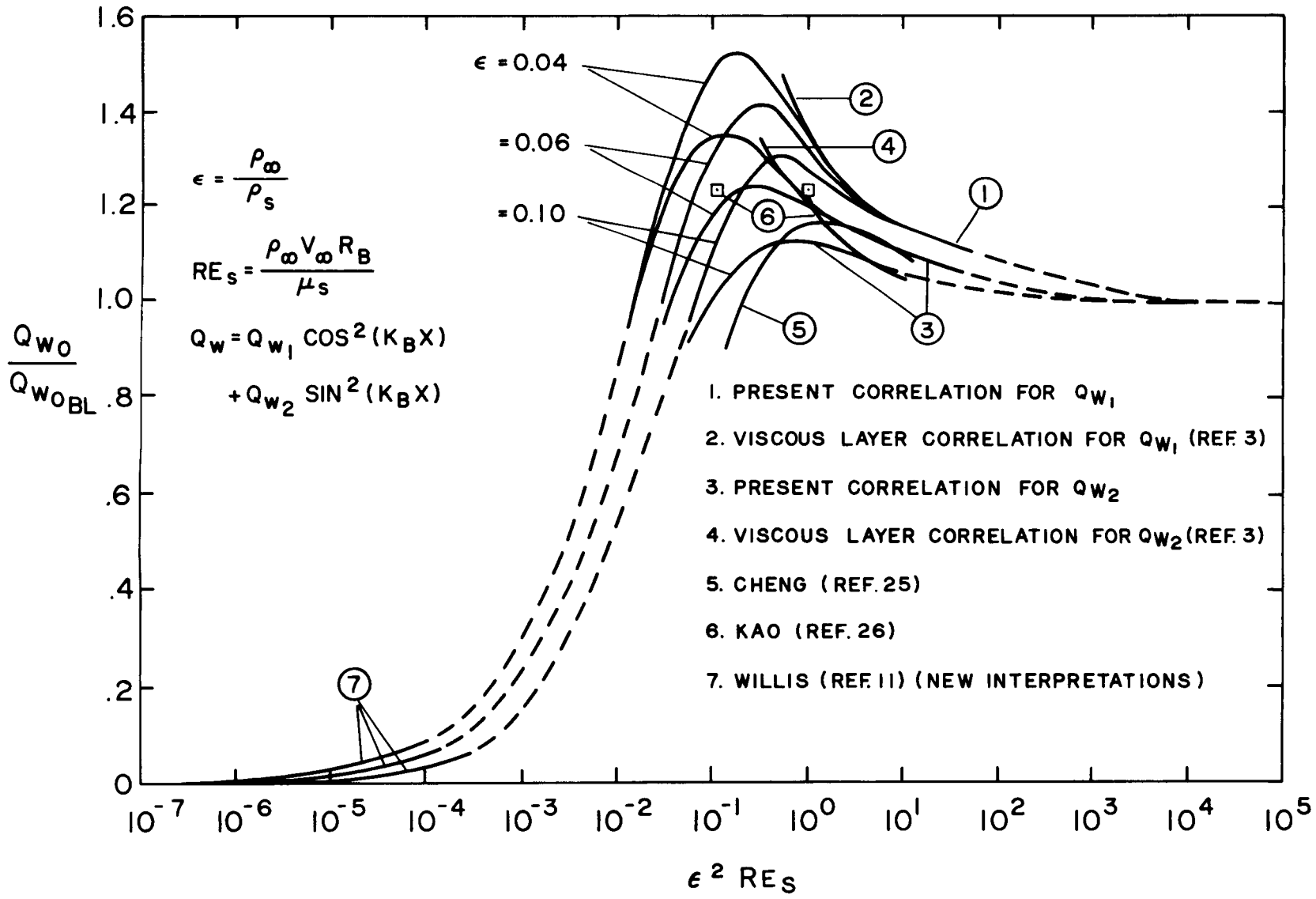

Figure 11. Normalized Heat Transfer

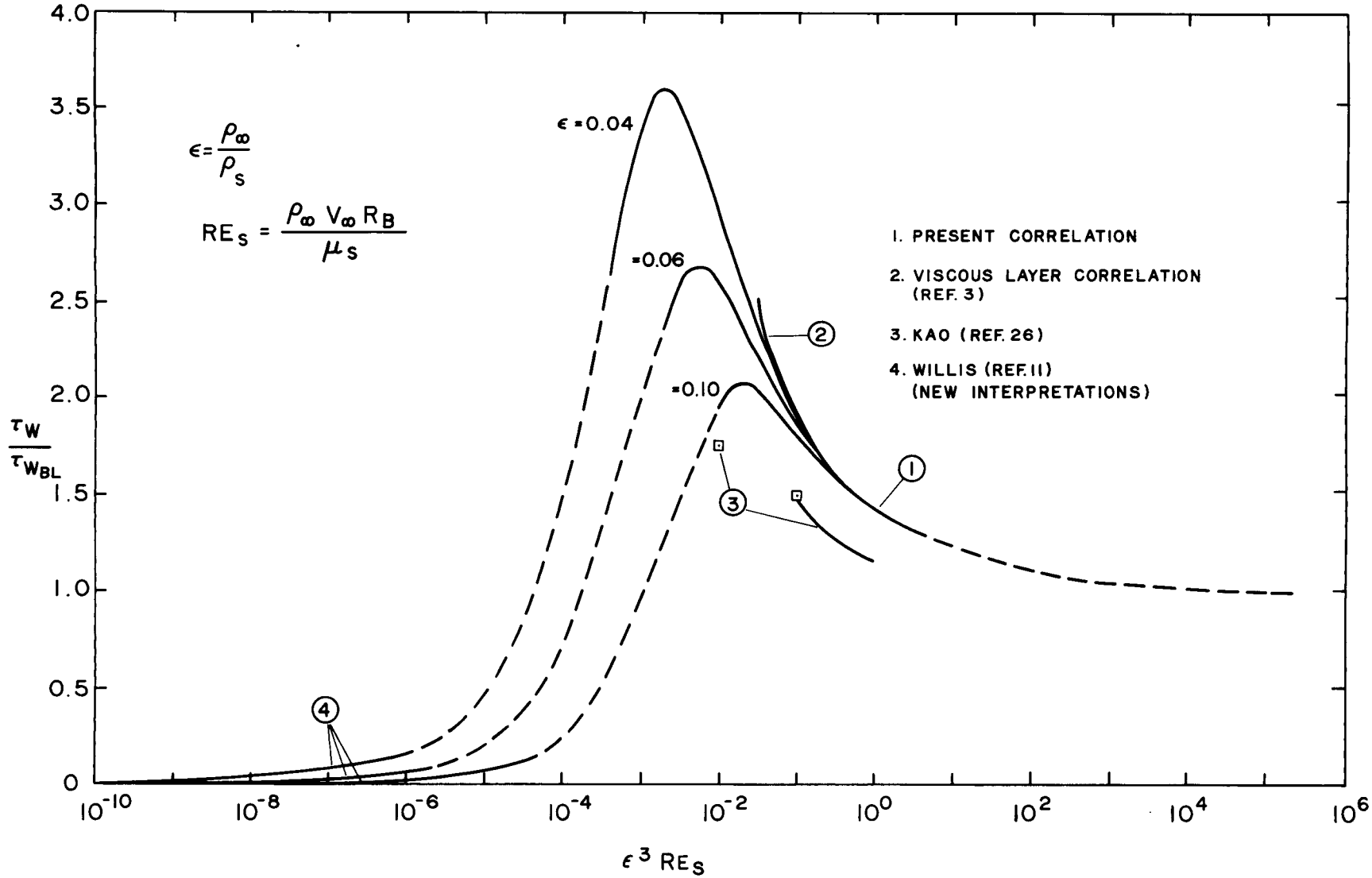

Figure 12. Normalized Skin Friction

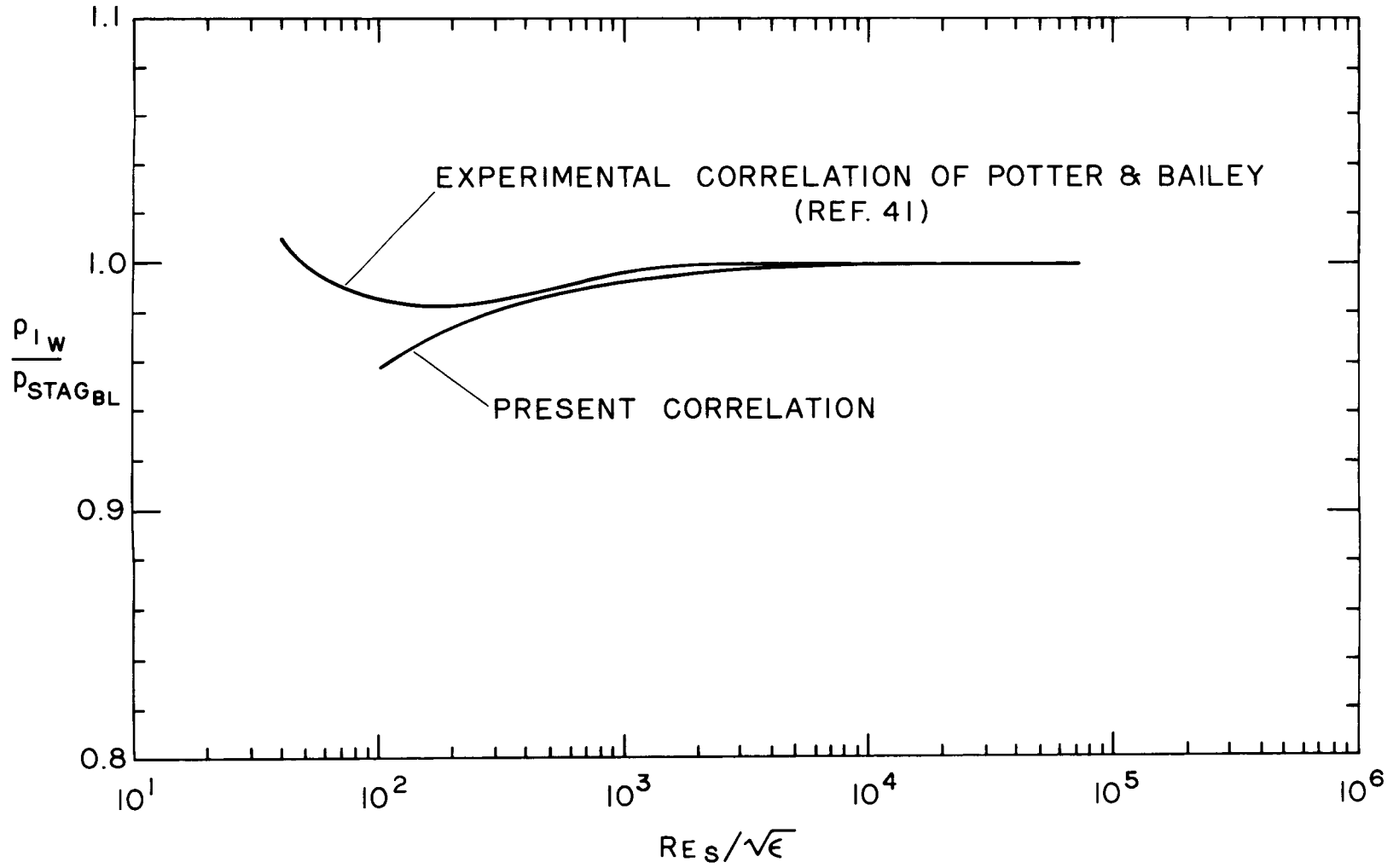

Figure 13. Normalized First Component of Pressure

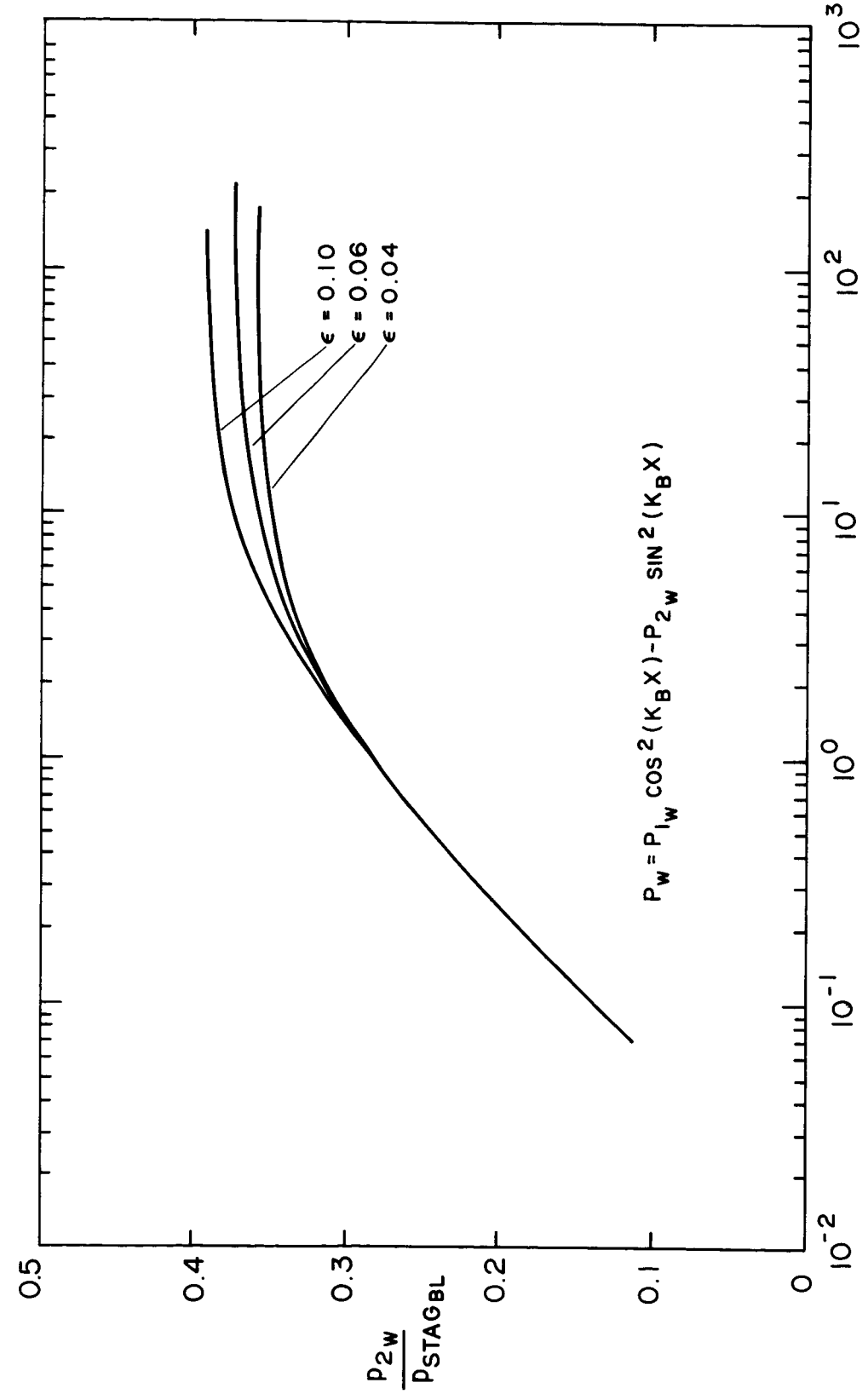

Figure 14. Normalized Second Component of Pressure

GENERAL ELECTRIC

SPACE SCIENCES LABORATORY
MISSILE AND SPACE DIVISION

TECHNICAL INFORMATION SERIES

AUTHOR	SUBJECT CLASSIFICATION	NO.
L. Goldberg	Hypersonic Low Reynolds Number Viscous Flow	R65SD50
		DATE: Dec., 1965
TITLE: THE STRUCTURE OF THE VISCOUS HYPERSONIC SHOCK LAYER		G. E. CLASS: I
		GOV. CLASS: U
REPRODUCIBLE COPY FILED AT MSD LIBRARY, DOCUMENTS LIBRARY UNIT, VALLEY FORGE SPACE TECHNOLOGY CENTER, KING OF PRUSSIA, PA.		NO. PAGES: 58

SUMMARY

In this paper, a unified, theoretical model of the hypersonic viscous shock layer is presented, which, in a self-consistent manner, covers the entire range of shock Reynolds number from 0 (50) to 0 (10^4), including the effects of mass transfer. At the lowest Reynolds numbers considered, merging of the fully viscous shock layer with the shock wave occurs, and at the highest Reynolds numbers, the boundary layer asymptote is approached.

In addition, in order to compare the new results obtained from this new system of equations and boundary conditions at high Reynolds numbers with those obtained from boundary layer solutions for precisely the same hypersonic flight conditions, the boundary layer equations have been reformulated by retaining only first order terms in the above equations, in addition to making the usual assumption of a thin boundary layer. These equations and the boundary conditions used are equivalent to the more usual boundary layer formulation.

Correlated results of the numerical solutions obtained on a high speed digital computer (IBM 7094) for both systems of equations with their appropriate boundary conditions are presented. The range of hypersonic flight conditions for which calculations were obtained include flight velocities from 10,000 ft/sec. to 25,000 ft/sec.; altitudes from 100,000 ft. to 350,000 ft.; shock Reynolds numbers from order 10 to order 10^4; surface temperatures from 800°R to 3500°R; and dimensionless mass transfer rate parameter f_w from 0 to -0.4. The correlations include non-similar heat transfer rates, skin friction and normal surface pressures.

KEY WORDS: Hypersonic; Low Reynolds Number; Merged Shock Layer; Skin Friction; Mass Transfer; Heat Transfer

BY CUTTING OUT THIS RECTANGLE AND FOLDING ON THE CENTER LINE, THE ABOVE INFORMATION CAN BE FITTED INTO A STANDARD CARD FILE.

AUTHOR: Leon Goldberg

COUNTERSIGNED: S. M. Scala, Manager
Theoretical Fluid Physics Section

Progress Is Our Most Important Product

GENERAL ELECTRIC